Two-Phase Microchannel Heat Sinks: Theory, Applications, and Limitations

Issam Mudawar
Boiling and Two-Phase Flow Laboratory (BTPFL),
Purdue University International
Electronic Cooling Alliance (PUIECA),
Mechanical Engineering Building,
585 Purdue Mall,
West Lafayette, IN 47907

Boiling water in small channels that are formed along turbine blades has been examined since the 1970s as a means to dissipating large amounts of heat. Later, similar geometries could be found in cooling systems for computers, fusion reactors, rocket nozzles, avionics, hybrid vehicle power electronics, and space systems. This paper addresses (a) the implementation of two-phase microchannel heat sinks in these applications, (b) the fluid physics and limitations of boiling in small passages, and effective tools for predicting the thermal performance of heat sinks, and (c) means to enhance this performance. It is shown that despite many hundreds of publications attempting to predict the performance of two-phase microchannel heat sinks, there are only a handful of predictive tools that can tackle broad ranges of geometrical and operating parameters or different fluids. Development of these tools is complicated by a lack of reliable databases and the drastic differences in boiling behavior of different fluids in small passages. For example, flow boiling of certain fluids in very small diameter channels may be no different than in macrochannels. Conversely, other fluids may exhibit considerable "confinement" even in seemingly large diameter channels. It is shown that cutting-edge heat transfer enhancement techniques, such as the use of nanofluids and carbon nanotube coatings, with proven merits to single-phase macrosystems, may not offer similar advantages to microchannel heat sinks. Better performance may be achieved by careful optimization of the heat sink's geometrical parameters and by adapting a new class of hybrid cooling schemes that combine the benefits of microchannel flow with those of jet impingement.
[DOI: 10.1115/1.4005300]

Keywords: microchannel, flow boiling, high flux

1 Introduction

1.1 Background. For several decades, flow boiling in small diameter channels has been recognized as an effective means for dissipating heat at very high rates [1]. To dissipate heat from planner surfaces, flow boiling can be achieved inside multiple parallel channels that are formed in a high conductivity substrate, a "microchannel heat sink."

Single-phase microchannel heat sinks have been explored quite extensively, especially in conjunction with electronics cooling [2–12]. These devices are very compact and lightweight, and their thermal merits are readily recognized for laminar flow, where the heat transfer coefficient is inversely proportional to hydraulic diameter; very high heat transfer coefficients can be achieved simply by using very small diameters. However, single-phase microchannel heat sinks intended for high flux situations produce high pressure drop and, because they rely on sensible heat rise to achieve the cooling, a large temperature gradient in the direction of fluid flow.

Two-phase microchannel heat sinks offer several advantages over their single-phase counterparts. First, they can achieve far greater heat transfer coefficients by utilizing the coolant's latent heat. This means a far smaller coolant flow rate is required to dissipate the same amount of heat as that of a single-phase heat sink, which helps to reduce coolant inventory for the entire cooling system. Additionally, by relying on mostly latent heat transfer, two-phase heat sinks provide better axial temperature uniformity, maintaining temperatures close to the coolant's saturation temperature.

However, two-phase microchannel heat sinks are not without shortcomings. In the earliest published studies addressing both the detailed thermal design of two-phase microchannel heat sinks and their limitations, Bowers and Mudawar [13–15] investigated flow boiling of R-113 in two different heat sinks containing circular cooling passages. The first heat sink featured 2.54-mm diameter "minichannels," while the second contained "microchannels" 0.51-mm in diameter. As shown in Fig. 1, while the microchannel heat sink did provide superior cooling performance, its pressure drop escalated rapidly following the initiation of boiling. This increase is the result of axial acceleration of the flow caused by a reduction in two-phase mixture density. This acceleration both increases the frictional pressure drop and introduces a second, accelerational pressure gradient. High pressure drop also can cause significant variations in the properties of the vapor and liquid. These variations are sometimes responsible for appreciable *compressibility* (specific volume variations of vapor and liquid with pressure) and *flashing* (vapor and liquid enthalpy variations with pressure); both of which increase the likelihood of *two-phase choking*. Because it can occur at much lower flow velocities in a two-phase mixture than in pure liquid or vapor flows [13–17], choking can be a serious limitation to cooling performance when using very small diameters. This point to the need for reliable predictive tools for the design and performance assessment of two-phase microchannel heat sinks.

Another obstacle to the implementation of two-phase microchannel heat sinks is the relatively limited understanding of transport behavior, which is caused by the difficulty diagnosing interfacial behavior in small channels. Other than high-speed video imaging and close-up photography, it is quite difficult to implement sophisticated two-phase flow instrumentation that is commonly used to characterize macrochannel flows [18].

1.2 Objectives of Study. The primary objectives of this paper are to (a) discuss the history and applications of two-phase

Contributed by the Electronic and Photonic Packaging Division of ASME for publication in the JOURNAL OF ELECTRONIC PACKAGING. Manuscript received July 11, 2011; final manuscript received September 30, 2011; published online December 8, 2011. Assoc. Editor: Giulio Lorenzini.

microchannel heat sinks, (b) explore the physics of flow boiling in microchannels and predictive tools for incipient boiling, pressure drop, two-phase heat transfer coefficient and critical heat flux (CHF), and (c) discuss means for enhancing the heat transfer performance of microchannel heat sinks.

It is important to emphasize that this paper is by no means a comprehensive literature survey but a summary of the author's own experiences and vision on this topic based on over 30 years of research he conducted first at the Massachusetts Institute of Technology (MIT) Energy Laboratory and Gas Turbine Laboratory in the late 1970s and early 1980s, since the mid-1980s at the Purdue University International Electronic Cooling Alliance and Boiling and Two-Phase Flow Laboratory (BTPFL), and during the last 7 years at the Rolls-Royce Purdue University Technology Center in High Mach Propulsion and the Purdue Hydrogen Systems Laboratory.

2 History and Applications

Many recent publications cite the work by Tuckerman and Pease [2] as the first study addressing the use of microchannel heat sinks. While this may be the case for electronics cooling, microchannel heat sinks have been in use much earlier and in a large variety of applications. Following are examples of key applications of two-phase microchannel heat sinks *other than* conventional electronics cooling.

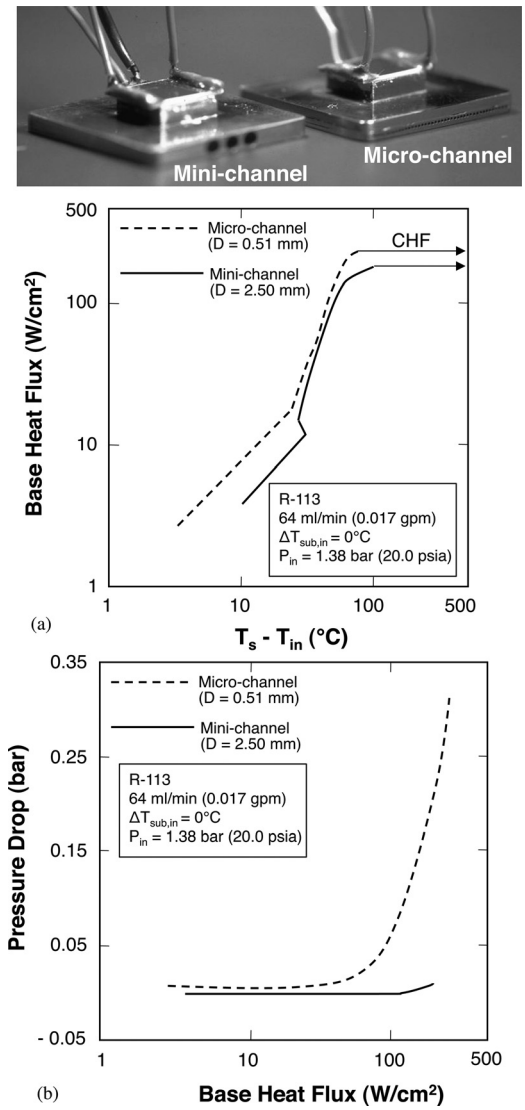

Fig. 1 Comparisons of (*a*) boiling curves and (*b*) pressure drop characteristics for microchannel and minichannel heat sinks with identical inlet conditions using R-113. (Adapted from Bowers and Mudawar [13])

2.1 Turbine Blades. Directly exposed to combustion products in a turbine engine, turbine blades encounter extreme temperatures, while having to endure very high stresses. The quest for greater efficiencies in modern turbines has lead to higher turbine inlet temperatures, creating the need for effective blade cooling schemes. Air cooling has been used in a variety of ways to achieve this goal, by internal forced convection within the blade, and by film and transpiration cooling. Liquid cooling has also been attempted in a few configurations, especially single-phase forced convection [19].

During the 1970s, the U.S. Department of Energy (DOE) initiated an aggressive high-temperature turbine program that was aimed at exploiting the merits of water cooling the turbine blades. Much of this program was based on a study by General Electric Company [20,21] that promised significant power plant combined-cycle efficiency improvements by increasing the firing temperature to 1650 °C. Aside from the efficiency improvements, a key goal was to enable the utilization of coal-derived and residual petroleum fuels. These initial studies pointed to a need to greatly decrease turbine blade temperatures in order to prevent hot corrosion effects in such a highly corrosive environment. Hot corrosion could be largely prevented if the blade surface temperature is maintained below 540 °C. Since air film and transpiration cooling techniques cannot maintain blade surface temperature in industrial turbines below 870 °C, only water cooling was deemed effective at achieving the 540 °C limit [20,21].

Much of the DOE blade water-cooling work was performed during the 1970s and early 1980s at the MIT Gas Turbine Laboratory. This work was focused primarily on water flow boiling to achieve the highest possible cooling rates and lowest blade surface temperatures. Studies first addressed flow boiling phenomena and CHF in a single rotating U-tube simulating water flow inside a single millimeter-sized turbine cooling passage [19]. By the late 1970s, focus shifted to a new concept involving cooling along small passages that supplied water radially outward through the blade but allowed the vaporized mixture to exit at the blade tip. As shown in Fig. 2, a series of small passages are formed around the blade perimeter. The water is driven through the blade mostly by centrifugal forces, while Coriolis forces cause the water to form into a thin layer along one side of the passage. Modifying the shape of the passages from circular to oval provides greater coverage of the passage perimeter with liquid and more effective overall blade cooling. Mudawar and El-Masri [22] emphasized the need to optimize the placement of cooling passages in order to minimize thermal resistance between the blade surface and wetted portion of the cooling passage perimeter. Mudawar et al. [23] and Mudawar and El-Masri [24] performed experiments to determine the influence of engine and coolant operating conditions on incipient boiling and CHF and developed a theoretical model for CHF that was based largely on the effectiveness of Coriolis forces at maintaining sufficient liquid flow along the wetted portion of the flow passage. CHF increased with increases in pressure and/or rotational speed. Their studies showed that it is possible to dissipate as much as 4500 W/cm^2 in industrial turbines by capitalizing upon the merits of both centrifugal and Coriolis forces in a small passage.

2.2 Fusion Reactor Blankets. Modern fusion reactors are based on the "tokomak" concept of magnetic containment where the plasma is confined in a donut-shaped vacuum vessel [25]. A mixture of deuterium and tritium, both hydrogen isotopes, is heated to over 150 million °C to form a hot plasma. A combination of strong magnetic fields that are produced by superconducting

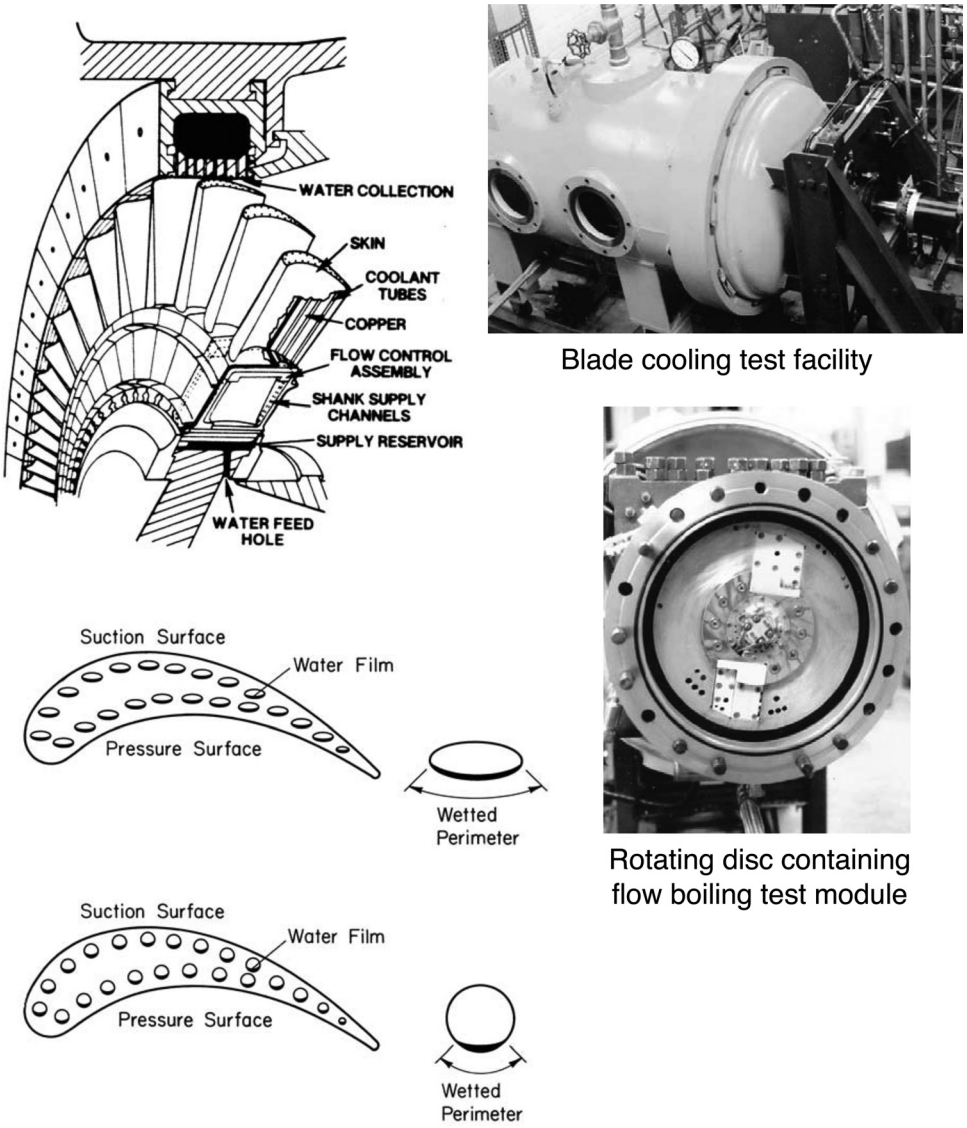

Fig. 2 Two-phase water cooling of turbine blades using open-tipped cooling passages. (Adapted from Mudawar et al. [23,24])

coils that surround the vessel and an electrical current through the plasma keeps the plasma away from the walls.

The fusion reactor blanket is one of the most critical components of a fusion reactor, because it extracts fusion power for generating electricity from the reactor's core. The "first-wall" of the reactor is the wall of the blanket directly facing the fusion plasma. This wall is exposed to extremely high heat fluxes and neutron loads from the plasma. To endure these conditions, the first wall consists of thin outer panels made from a high conductivity material such as beryllium or copper to protect the surface from the plasma particles and is cooled from behind by many small coolant channels as depicted in Fig. 3(*a*). Heat fluxes encountered in these cooling channels are among the highest ever reported in the literature, with some exceeding 10^4 W/cm^2 [26]. Since these heat fluxes exceed the CHF attainable with common flow boiling systems, the ability to greatly increase and predict the magnitude of CHF is of paramount importance to fusion reactor blanket design.

To tackle the extreme heat loads in fusion reactor blankets, Mudawar and Bowers [27] experimentally explored water flow boiling conditions that insure operation in the nucleate boiling regime safely below CHF. A combination of very high mass velocity ($G = 120{,}000$ kg/m^2·s), small tube diameter ($D = 0.406$ mm), and high subcooling yielded the highest CHF of 27,600 W/cm^2 ever reported in the literature for a uniformly heated tube, eclipsing the prior record of 22,800 W/cm^2 achieved by Ornatskii and Vinyarskii [28] in the mid-1960s.

Using the experimental database compiled by Mudawar and Bowers, Hall and Mudawar [29] developed a CHF correlation for extreme heating conditions, such as those encountered in fusion reactor blankets. They showed that high CHF could be achieved by increasing mass velocity, decreasing tube diameter, increasing inlet subcooling, and/or operating at elevated pressures. Figure 3(*b*) shows relatively low CHF values are achieved near atmospheric pressure and the critical pressure, and CHF is highest around 70 bar. Notice also the monotonic increase in CHF with increased subcooling. The upper and lower boundaries in Fig. 3(*b*) represent an inlet temperature equal to the triple-point temperature and an outlet quality equal to zero, respectively.

2.3 Rocket Engines. The walls of thrust chambers in modern liquid rocket engines encounter very high pressures and temperatures. In hydrogen/oxygen liquid rocket engines, the walls are cooled by hydrogen flowing at high flow rate through rectangular microchannels as illustrated in Fig. 4(*a*). Wall cooling effectiveness is paramount to the life of the thrust chamber, which can be

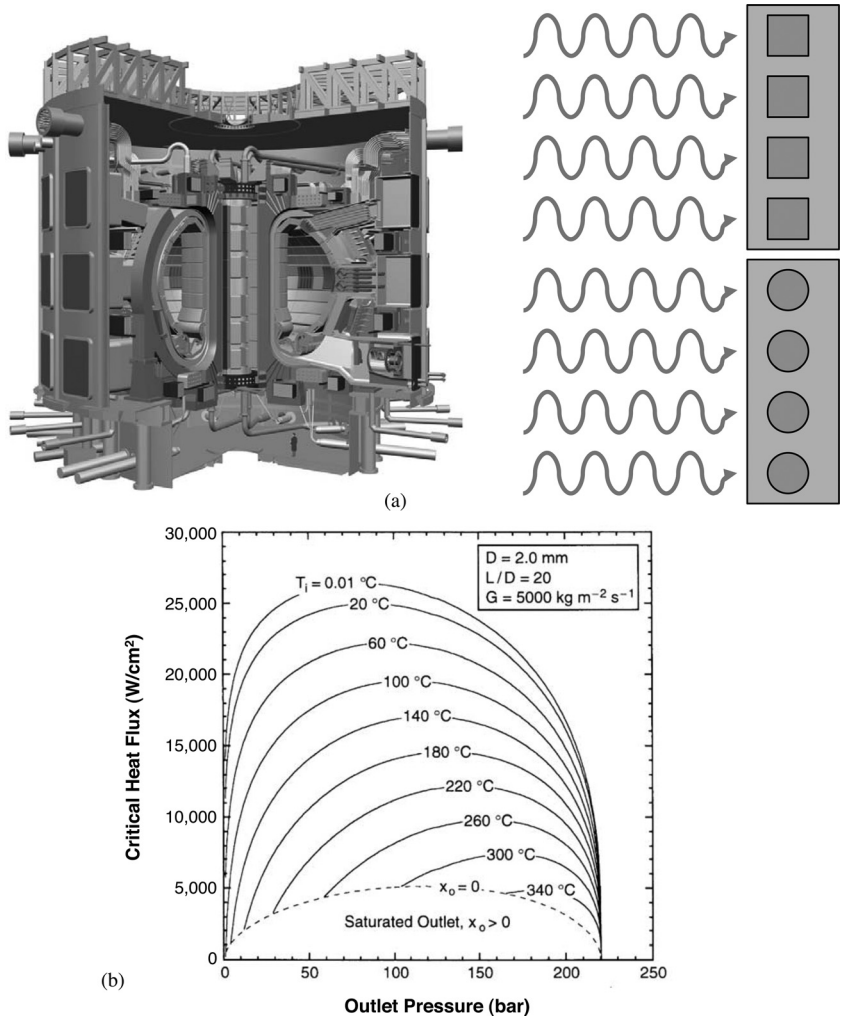

Fig. 3 (*a*) International thermonuclear experimental reactor (ITER) [25] and schematics of microchannel cooling of first-wall of fusion reactor blanket. (*b*) Variation of CHF for water flow boiling through single tube with inlet temperature and outlet pressure based on Hall and Mudawar's high-flux inlet conditions correlation [29].

nearly doubled, if the wall temperature is reduced by 50–100 °C [30].

For a given heat transfer coefficient h inside the coolant channel, the effectiveness of the metal wall between microchannels (ratio of heat transfer with, compared to without the wall) of thickness W_w and conductivity k_w can be approximated as $\varepsilon = (2k_w/hW_w)$ [31]. This implies high cooling performance can be achieved by using a large number of closely spaced thin walls, provided the flow in the channels is not severely restricted. This amounts to using many closely spaced channels—microchannels—that are separated by thin walls. A high channel height-to-width (H_{ch}/W_{ch}) ratio both enables maximum utilization of the wall's fin effect (i.e., causing the wall to behave as an infinite fin) and serves to prevent high pressure drop in the cooling channels. This explains a recent trend in cooling wall design, where rocket engines containing channels with $H_{ch}/W_{ch} \sim 8$, Fig. 4(*b*), are used instead of the conventional ratio of about 2 [32].

Depending on the type of coolant and operating conditions of the rocket engine, flow boiling may or may not be desired. Flow boiling does offer the advantage of greatly enhancing cooling performance and reducing wall temperature. However, CHF inside the cooling channel is a primary concern and must be ascertained and prevented. Flow boiling CHF in this application is complicated by the channel's rectangular shape, aspect ratio and, most importantly, curvature.

Curvature is known to enhance flow-boiling CHF from concave heated walls. Gambill and Green [33] and Gu et al. [34] correlated CHF with centrifugal acceleration to the one-fourth power, drawing on the pool boiling correlation proposed by Zuber et al. [35], which contains Earth's gravity raised to the one-fourth power. Sturgis and Mudawar [36,37] performed photomicrographic studies of vapor coalescence along the concave surface of a 5.0 mm high by 2.5 mm wide rectangular channel. Figure 5 depicts vapor being pulled inward as liquid is pushed outward by the centrifugal force, removing the vapor from the concave wall, especially near the leading edge of the heated wall. Farther downstream, vapor is removed from the concave wall, fragmented and distributed throughout the cooler bulk flow, where it is better able to utilize the bulk subcooling. CHF was enhanced by up to 60% for a centrifugal force equivalent to 315 Earth g_es. Sturgis and Mudawar [36] proposed a theoretical model for the influence of channel curvature on near-saturated flow boiling in small channels, which was based on the *Interfacial Lift-off Model* used to predict CHF in both pool boiling [38,39] and flow boiling along flat surfaces [40–43].

2.4 Avionics. Cooling of avionics onboard modern military and commercial aircraft is achieved inside avionic enclosures, rectangular chasses that serve the multiple purpose of mechanical

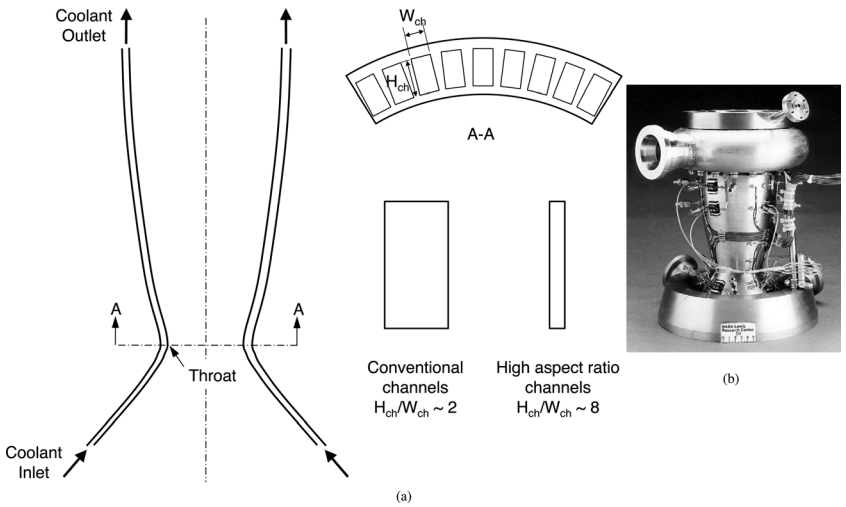

Fig. 4 (*a*) Schematic of rocket engine microchannel cooling. (*b*) Photograph of NASA combustion chamber utilizing high aspect ratio cooling channels [32]

mounting of circuit boards and electrical interconnect, in addition to the cooling. As shown in Fig. 6(*a*), an avionics enclosure contains several closely packed modules that contain the circuit boards. In the majority of today's avionics, each module houses two circuit boards mounted back-to-back against a thermally conducting substrate. The substrate routes the heat dissipated by the circuit boards into the top and bottom heat exchange walls of the avionics enclosure. The heat is rejected to air that is bled directly from the compressor of the jet engine or bypassed from the engine's fan.

Because of the long thermal path from device to the air, a conventional 13.66 cm × 16.28 cm × 1.51 cm thick (5.38 in. × 6.41 in. × 0.59 in.) edge air-cooled module can dissipate no more than about 40 W. However, by the early 1990s, device and packaging developments in military aircraft resulted in substantial increases in heat dissipation at the module level. Edge air cooling was replaced by a new generation of liquid cooled modules, where the conducting substrate was replaced by a hollowed, liquid-cooled metallic frame. Using polyalphaolafin (PAO) as single-phase coolant, the heat dissipation capability per module was increased to about 200 W [44].

A more effective means to improving the cooling performance of avionic modules is to allow the coolant to make direct contact with the device and undergo phase change. Mudawar et al. [45] developed a clamshell-type module, *BTPFL-C1*, which featured an open inner cavity inside with two circuit boards attached to the module's inner walls. Dielectric coolant FC-72 was supplied into the cavity and allowed to flow undirected at very low speed before exiting the module to an external conditioning flow loop. They demonstrated that this module could dissipate over 820 W, four times the cooling rate of the PAO module.

Jimenez and Mudawar [46] later incorporated two-phase microchannel cooling to further enhance the thermal performance of their earlier clamshell module. As shown in Fig. 6(*b*), the new *BTPFL-C2* module housed two circuit boards that were separated by a flow distribution plate. The coolant passed through parallel narrow microchannels formed between the distribution plate and the surfaces of the devices. Capitalizing upon the merits of microchannel flow boiling, the BTPFL-C2 was able to dissipate over 3000 W using Fluorinert FC-72, corresponding to a mild flow rate of 0.051 kg/s (0.50 gpm), 40.5 °C subcooling and a pressure drop of only 2.8 kPa (0.41 psi).

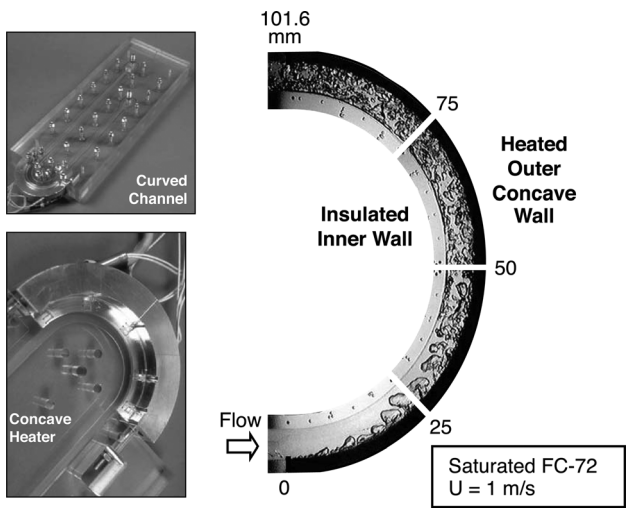

FIG. 5 Vapor removal from concave heated wall of small rectangular channel by centrifugal forces [36]

2.5 Hybrid Vehicle Power Electronics. The automobile industry is presently witnessing unprecedented interest in the development of new electric propulsion systems in an effort to transition from conventional engines to economical combustion engine hybrid vehicles in the near term and to fuel cell vehicles in the long term. Evidence of this transition can be found in the FreedomCAR and Fuel Partnership programs spearheaded by DOE [47].

To successfully implement power electronics and electric machines into hybrid and fuel cell vehicles, Fig. 7(*a*), various thermal characteristics and performance targets must be met. Thermal management will play a paramount role toward achieving those targets, but several barriers must first be overcome. For example, existing thermal management techniques in automobiles are not adequate for dissipating high heat fluxes, while limiting the operation of silicon-based electronic components to a temperature of less than 125 °C. Additionally, current components are generally both bulky and heavy, resulting in the need for additional structural support and increased use of parasitic power. Therefore, new liquid cooling technologies are sought for power electronics (and also motors) that can tackle higher power densities and reduce volumes and weights.

Cooling of the vehicle's power electronics is achieved by channeling the heat from the chip through different layers of materials separating the chip from the liquid coolant. To achieve the aforementioned thermal goals, two-phase microchannel cooling can be implemented as illustrated in Fig. 7(*b*). One possible type of

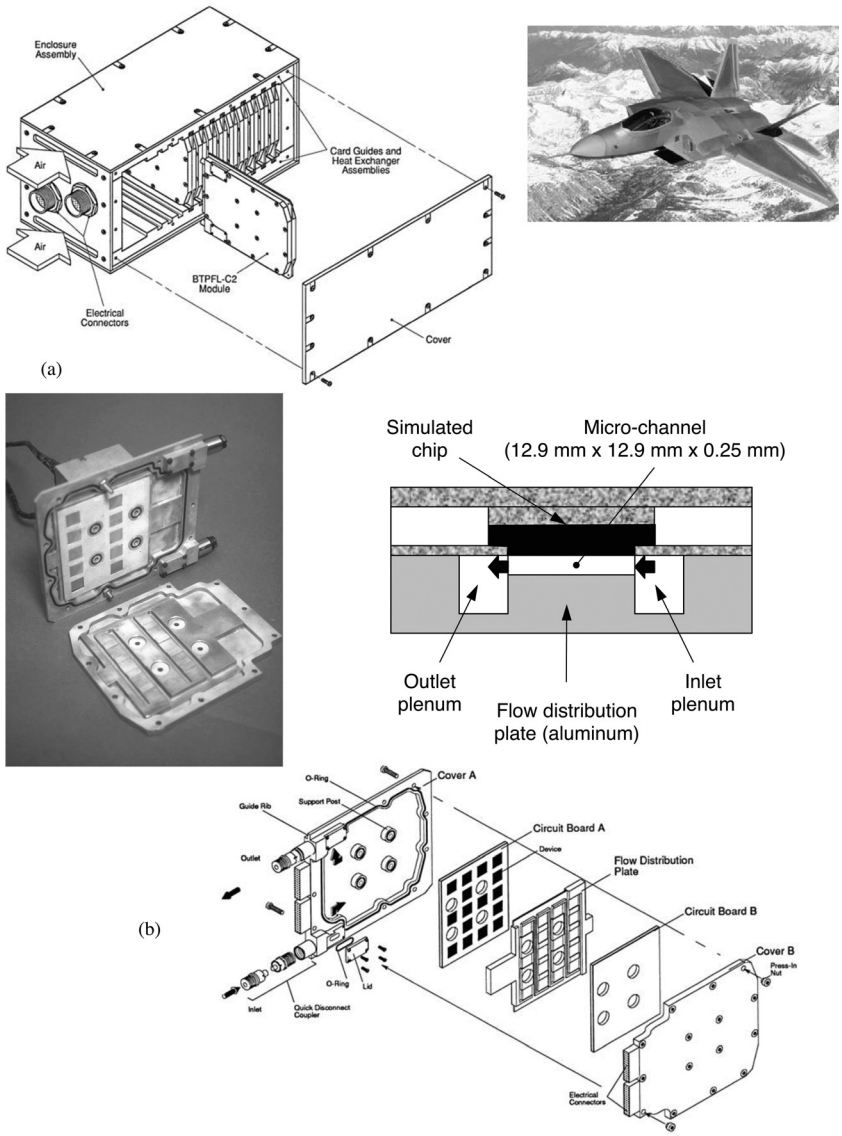

Fig. 6 (*a*) Schematic of avionics enclosure housing multiple two-phase clamshell cooling modules [45]. (*b*) Construction of microchannel cooling module [46]

coolant is a refrigerant such as R134a that can be circulated in a pump-assisted subloop containing the microchannel hardware. The subloop would tap into the vehicle's primary refrigeration loop and also reject the heat to the vehicle's air-cooled condenser. Another possibility is to use a dielectric coolant such as HFE 7100 with a separate cooling loop. Details of these loop options can be found in Ref. [48].

2.6 Hydrogen Storage. Recently, hydrogen has attracted significant attention as a promising and sustainable energy solution for mobile systems. Aside from being the most abundant element on Earth, hydrogen is lightweight, has high energy content per unit mass and produces water as a result of oxidation. This means that effective use of hydrogen can ensure a virtually unlimited and environmentally safe source of energy.

Storage volume is one of the major challenges to overcome before hydrogen can become a viable fuel for automobiles. Though hydrogen has high energy content by weight (three times that of gasoline), its energy content by volume is only one-tenth that of gasoline [49]. This poses major storage volume problems in automotive and other mobile systems having stringent volume constraints.

Hydrogen can be stored either in gaseous form, liquid form, or in the form of reversible compounds with certain metals or alloys. One form of solid-state hydrogen storage is in high-pressure metal hydrides (HPMHs), such as $Ti_{1.1}CrMn$, which are metal compounds or alloys that react reversibly with hydrogen to form hydrides. One of the advantages of HPMHs is their ability to store the hydrogen at up to 700 bar at moderate temperatures of less than 100 °C [50]. However, they are known to release very large amounts of heat when the hydrogen is supplied into the storage system at the filling station. The rate of the ensuing "hydriding" reaction associated with the hydrogen filling depends on the temperature of the metal hydride. It is, therefore, very important that the released heat be removed efficiently and why the most important component of a hydrogen storage system using HPMHs is the heat exchanger [50]. Poor thermal properties of HPMH powder render the design of an efficient heat exchanger quite elusive. Another challenge is to reduce the volume of all heat exchanger parts to increase storage capacity for the HPMH.

Recently, Visaria et al. [51,52] and Mudawar [53] developed several heat exchanger designs to tackle the heat removal from HPMH hydrogen storage systems for automobiles. The most recent of these consists of a series of identical heat exchange modules that are cooled by passing a coolant such as Dex-cool from a cooling tube. As shown in Fig. 8, each module consists of aluminum base and cover plates that are brazed together. The base plate

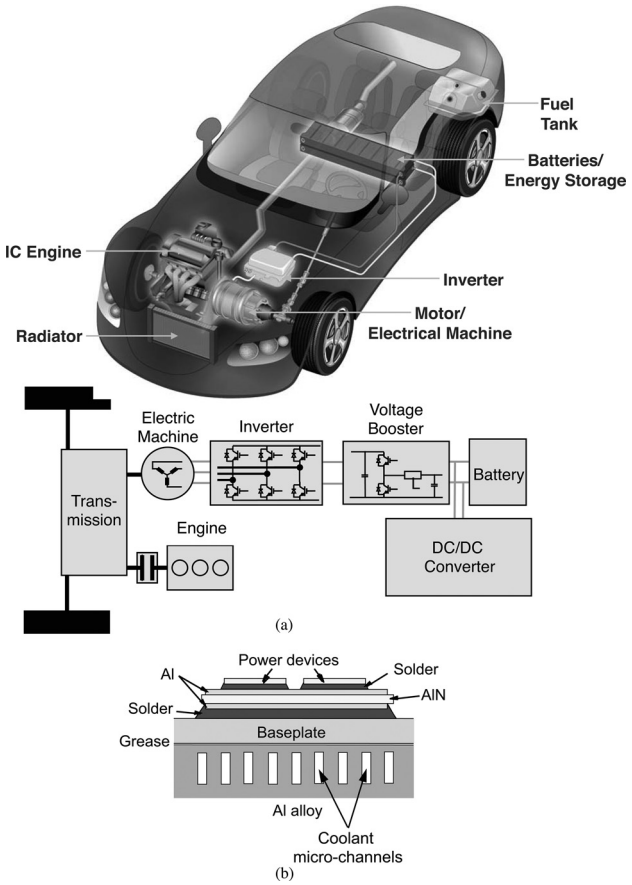

Fig. 7 (*a*) Propulsion system components for hybrid vehicle [47,48]. (*b*) Microchannel cooling of electronic power device

is grooved with serpentine microchannels for the coolant flow, and both the base and top plates feature external circular fins. The HPMH is filled into cavities between the fins on both sides of the module. The effectiveness of this heat exchanger design is derived mostly from the high heat transfer coefficients made possible by the serpentine microchannel. Small coolant passage cross-sectional area greatly reduces the volume of both aluminum and coolant relative to the HPMH inside the storage pressure vessel. This is a further example of an application that can benefit greatly from the thermal attributes of microchannel flow.

2.7 Refrigeration Cooling. While modern electronic and power devices have witnessed a significant increase in heat dissipation rate, the maximum allowable temperature in most applications has remained fairly constant or increased by a very modest amount. In any liquid cooling application, the temperature of the device increases with increasing heat dissipation rate for a fixed coolant temperature. This relationship could bring the device temperature above the maximum limit when dissipating high heat fluxes. Maintaining acceptable temperatures in these situations can be accomplished by reducing the temperature of the liquid coolant to compensate for the increasing heat flux. This trend would ultimately require coolant temperatures below ambient, which necessitates the use of a refrigeration system to sustain the cooling.

Various refrigeration cooling schemes have been explored [54,55]. Of those, vapor compression systems were deemed most practical because of their relatively high cooling capacity at temperatures of interest [56–58]. Refrigeration cooling can be implemented in two different configurations that can both accommodate microchannel heat sinks. In the first *direct-refrigeration-cooling* configuration, Fig. 9(*a*), the microchannel heat sink can serve as evaporator in the vapor compression cycle. Here, the refrigerant is used as coolant for the heat-dissipating device. The second *indirect-refrigeration-cooling* configuration involves using two fluid loops as depicted in Fig. 9(*b*). Heat from the device is rejected via a microchannel heat sink to a primary coolant circulating through a pumped liquid loop that rejects the heat via a heat exchanger to a refrigerant flowing in a separate vapor compression loop. These configurations produce two drastically different types of flow boiling inside the heat sink, *saturated* and *subcooled*, respectively.

In the direct-refrigeration-cooling configuration, a refrigerant such as R134a enters the microchannel evaporator as a two-phase mixture and exits as saturated or superheated vapor as required by the compressor. The refrigerant undergoes rapid change of phase into a high void fraction mixture inside the evaporator, resulting in mostly slug and annular flow. Consequently, two-phase pressure drop and heat transfer models for the microchannel evaporator are based mostly on these regimes [59–65].

The separate primary coolant loop in the indirect-refrigeration-cooling configuration provides great flexibility in attaining the desired microchannel heat sink's inlet conditions, and the coolant need not be maintained in a saturated state. In fact, the coolant is supplied to the heat sink in subcooled state with a thermodynamic equilibrium quality below zero. The quality increases along the microchannels but, because microchannel heat sinks are relatively short, subcooled boiling can prevail to the outlet. Because of the relatively small void fraction in subcooled boiling, both the pressure drop and heat transfer characteristics are categorically different from those for saturated boiling. Lee and Mudawar [66–69] developed design relations for pressure drop, two-phase heat transfer coefficient and CHF for the indirect-refrigeration-cooling configuration using HFE 7100 as primary coolant. They showed that, while the R134a direct-refrigeration-cooling configuration does yield very high heat transfer coefficients, its cooling performance is limited by low CHF [64,65]. Because of the ability to maintain subcooled conditions, indirect-refrigeration-cooling can yield much higher CHF values and is, therefore, far better suited for high-flux heat dissipation. Tests with this system yielded heat fluxes as high as 840 W/cm^2 with HFE 7100 without encountering CHF [70].

2.8 Thermal Control in Microgravity. With projected increases in scope, complexity and duration of future space missions, both power and heat dissipation demands are expected to rise. The success of these missions will depend largely on the ability to reduce the size and weight of all key thermal management subsystems. One means to achieving this goal is to reduce the surface area of heat exchange surfaces by replacing single-phase systems with two-phase systems, which can yield orders of magnitude enhancement in the heat transfer coefficient [71]. Small size and weight, minimal coolant inventory requirements, and the ability to produce very high evaporation and condensation heat transfer coefficients are all reasons why two-phase microchannel devices are expected to play a crucial role in future space mission.

Space missions span varying gravitational levels as illustrated in Fig. 10. Microgravity is important to the operation of satellites and Earth orbiting vehicles and stations. Future space missions will demand a strong understanding of the influence of Lunar to Martian reduced gravity environments. On the other hand, thermal systems in fighter aircraft must be able to handle relatively large body forces. Large density differences between liquid and vapor create buoyancy effects in the presence of any gravitational field. Therefore, the magnitude of the gravitational field can have a significant influence on two-phase fluid flow and heat transfer, especially CHF.

Zhang et al. [72] performed FC-72 flow boiling experiments in microgravity, Lunar gravity (0.16 g_e) and Martian gravity (0.38 g_e), conditions that were produced during parabolic maneuvers aboard NASA's KC-135 turbojet and Zero-G Corporation's Boeing

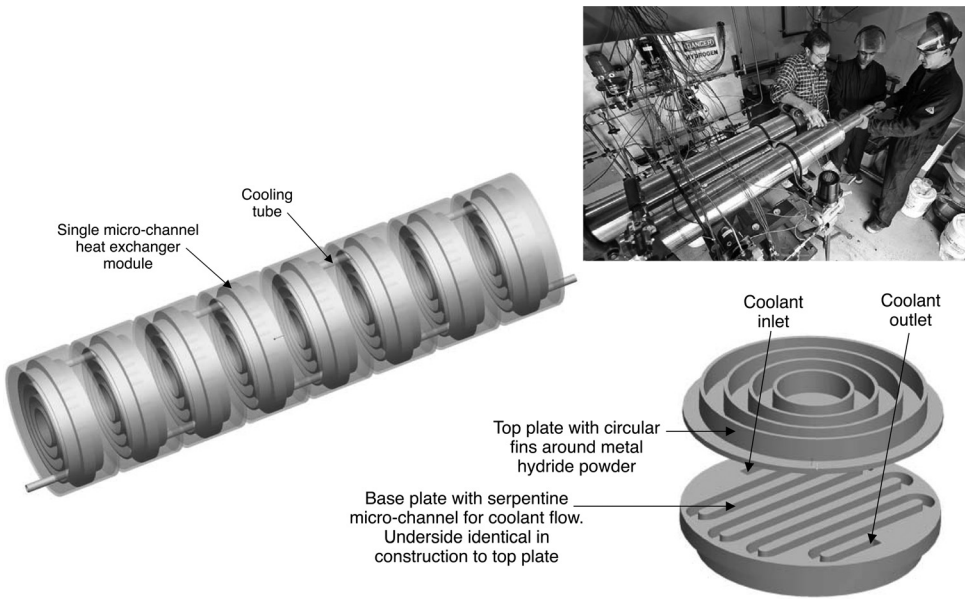

Fig. 8 Serpentine microchannel heat exchanger for HPMH hydrogen storage [53]

727-200. Vapor behavior was monitored along a 2.5-mm wide by 101.6-mm long heated wall of a rectangular channel with the aid of a high-speed video camera. Their observations and data trends were in general agreement with earlier microgravity studies by Saito et al. [73], Cochran [74], and Ma and Chung [75]. Figure 11 contrasts Zhang et al. CHF data variations with inlet liquid velocity for $1\,g_e$ and μg_e. While the effect of velocity on CHF in $1\,g_e$ is relatively mild, CHF at the lowest velocity in μg_e is only 50% of that in $1\,g_e$. The effects of buoyancy become negligible around 1.5 m/s, at which CHF values for $1\,g_e$ and μg_e appear to converge. This

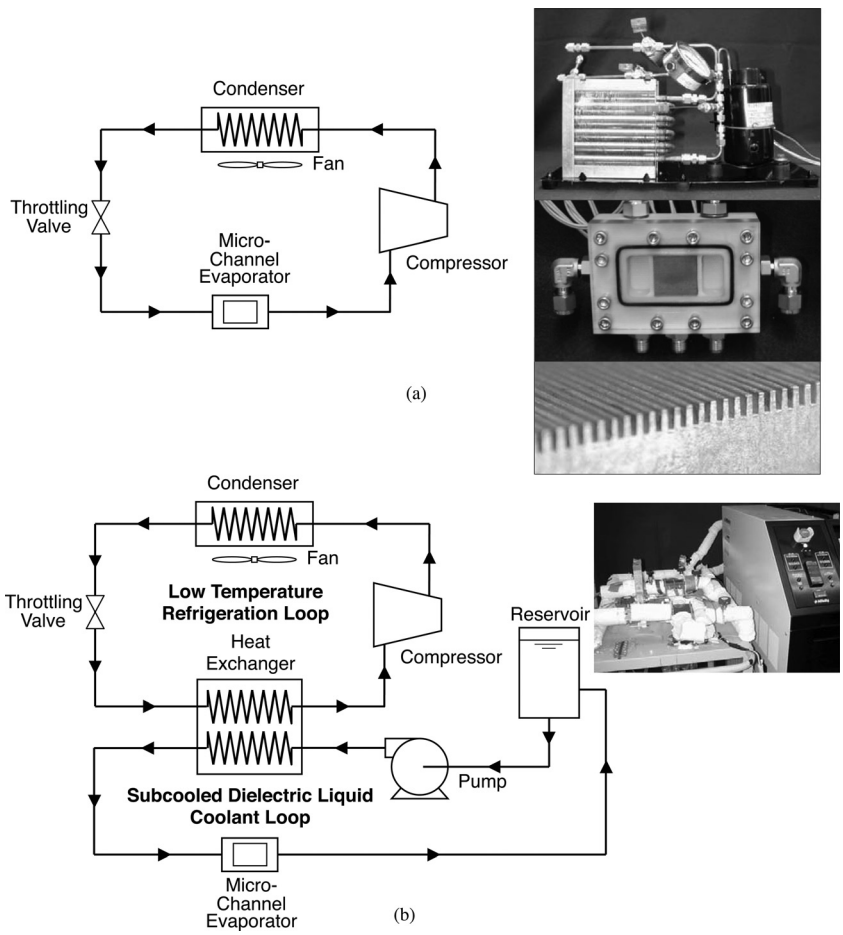

Fig. 9 (*a*) Direct-refrigeration-cooling and (*b*) indirect-refrigeration-cooling systems

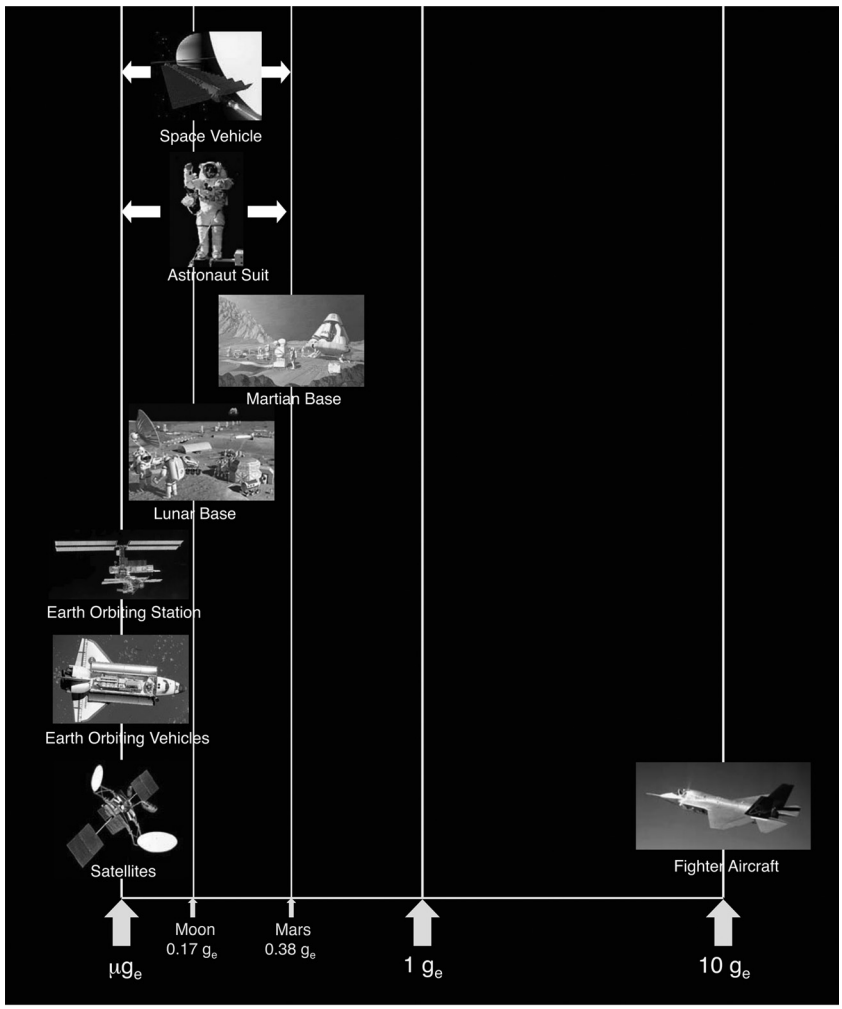

Fig. 10 Examples of systems demanding predictive models for effects of gravitational field on two-phase flow and heat transfer

convergence of CHF data has important practical implications to the design of space thermal management systems since, by knowing the velocity at which such convergence occurs, designers may be able to utilize the vast body of knowledge amassed from celestial two-phase studies to design reduced gravity thermal management systems with confidence, provided the liquid velocity exceeds the convergent value. Zhang et al. [76–78] developed a theoretical model to predict CHF in reduced gravity, and dimensionless criteria for determining the convergent velocity limit.

Aside from their well-known merits of small size and weight, minimal coolant inventory, and the ability to produce very high heat transfer coefficients, two-phase microchannel heat exchange

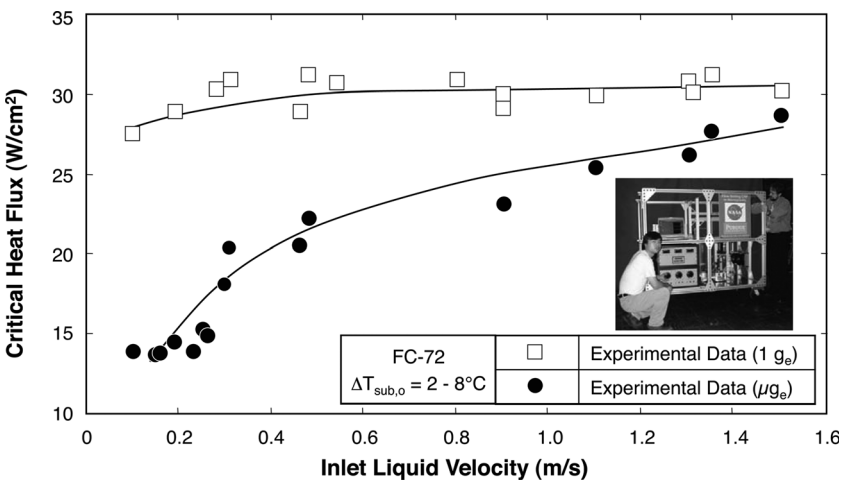

Fig. 11 CHF data for μg_e and horizontal 1 g_e flow boiling. (Adapted from Zhang et al. [72])

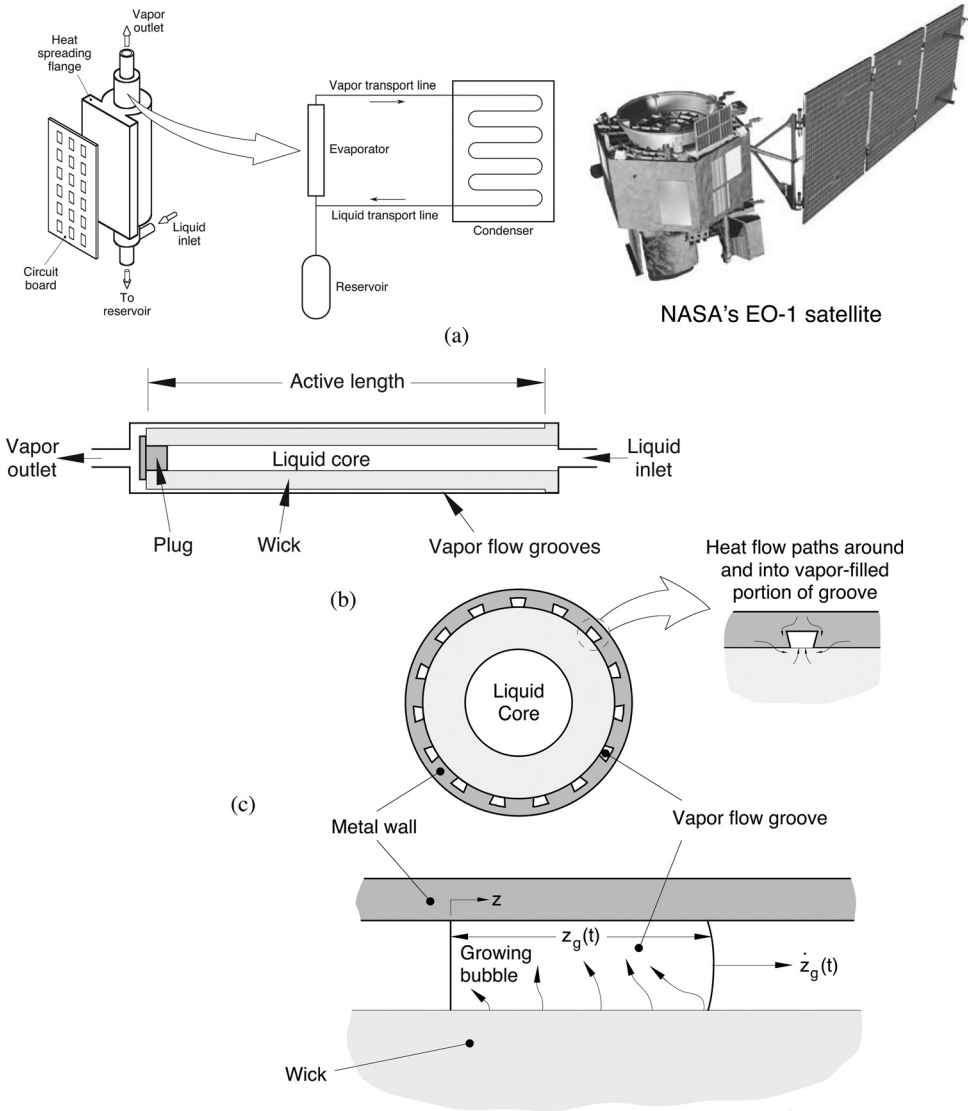

Fig. 12 (*a*) Basic CPL configuration and circuit board attachment to tubular CPL evaporator; (*b*) evaporator construction; and (*c*) evaporator cross-section and groove detail showing axial growth of first bubble during CPL startup. (Adapted from LaClair and Mudawar [80] and Cullimore [82])

devices offer additional crucial benefits to space systems. Because of their small hydraulic diameter, relatively high flow velocities are produced inside microchannels even when small coolant flow rates are used. Furthermore, phase change along the microchannel causes appreciable flow acceleration, with velocities vastly surpassing the typical 1.5 m/s convergence limit. These points to (1) the effectiveness of these devices at easily overcoming the detrimental effects of microgravity on CHF and (2) the ability to design these devices with confidence using fluid flow and heat transfer models derived from celestial studies.

2.9 Capillary-Pumped Loops. Satellites pose unique challenges to the design of a thermal management system for electronics. These challenges are mostly the result of operating environment, which influences every aspect of the heat acquisition, transport, and rejection. In most satellites, waste heat from electronic assemblies is transported to radiator panels that reject the heat by radiation to deep space. Because of the relatively long distances between electronic assemblies and radiator panels, conventional heat pipes fail to achieve the desired thermal transport task. Certain satellites also operate on a very limited "power budget" and are intended for 10 years or more of maintenance-free operation, which precludes the use of mechanical pumps [79,80].

Capillary pumped loops have been developed to fill the gap between conventional heat pipes and mechanically pumped liquid loops. A CPL is a two-phase system designed to transport heat over a length of up to tens of meters to reject heat from one or multiple heat sources. The working fluid is pumped passively by capillary forces developed in a wicked evaporator. As shown in Fig. 12(*a*), heat from the electronic sources is conducted to the outer wall of the evaporator. During normal operation, the working fluid enters into the evaporator in liquid state, where it extracts the waste heat by evaporation. The fluid exits the evaporator in vapor state and flows to the condenser that is attached to radiator panels, where it returns to liquid state. Excess fluid inventory in the CPL is handled by a reservoir, which may be thermally controlled to achieve the desired CPL saturation temperature and pressure.

Serving as the CPL's pump, the evaporator is the most critical component of the CPL, and microchannel flow plays a crucial part in maintaining the desired evaporator operation. The evaporator consists of a grooved cylindrical metal shell that encases a porous, annular wick as illustrated in Fig. 12(*b*). The incoming liquid occupies the central core of the evaporator and is drawn radially

outward through the wick by capillary forces. The liquid evaporates at the wick's boundary in the grooves—microchannels that are typically less than 1-mm wide—of the metal wall, where menisci are formed. The capillary pressure rise across these menisci is what drives the fluid throughout the CPL. The microchannels serve as vapor flow passages.

Reliable operation of a CPL requires that only liquid be present in the liquid transport line and reservoir line, and in the evaporator core and wick. This maintains liquid supply to the wick-microchannel boundary where evaporation takes place. However, any vapor or gas bubbles in the "liquid side" of the loop may eventually result in a serious failure mode termed *deprime* [81]. This is a key concern during the CPL startup, when the vapor microchannels are initially filled with liquid. Initial vapor bubble growth within the microchannels causes liquid acceleration that results in a differential pressure spike. The deprime will occur if the pressure spike is large enough to force vapor backward into the evaporator's liquid-saturated wick.

Recently, LaClair and Mudawar [82] constructed a transient 3D model to predict the initial bubble growth. They postulated that, after a bubble nucleates in one of the CPL's evaporator microchannels, subsequent vapor growth would favor evaporation into the initial bubble as illustrated in Fig. 12(*c*). During this vapor growth phase, liquid previously occupying the microchannel is displaced out of the evaporator and/or backward through the wick. This raises the pressure and, hence, the saturation temperature in the evaporator, which serves to suppress nucleation in other locations of the same microchannel or in other microchannels during the initial vapor growth phase. The model can be used to assess the influence of initial system superheat, microchannel shape and size, and wick material on bubble growth rate and, hence, the likelihood of a deprime.

Overall, the CPL represents an application utilizing microchannel flow in which the goal is to *suppress* initial bubble growth rate rather than promote flow boiling inside the microchannels.

3 Transport Phenomena in Two-Phase Microchannel Heat Sinks

3.1 How Predictable is Single-Phase Microchannel Flow? For some time, researchers were in disagreement over the validity of the Navier–Stokes and energy equations to single-phase microchannel flows. Those who questioned this validity based their thesis on disagreements between pressure drop measurements across microchannels and macrochannel predictive tools [83–86], others found macrochannel tools quite effective at predicting microchannel flows [87–89].

Qu et al. [90] further explored this issue by investigating flow development and pressure drop both experimentally and computationally for adiabatic single-phase water flow in a single 222 μm wide, 694 μm deep, and 12 cm long microchannel, Fig. 13(*a*), at Reynolds numbers from 196 to 2215. The velocity field was measured using the micro-PIV system depicted in Fig. 13(*b*). A three-dimensional computational model of the flow was constructed to predict liquid velocity in both the developing and fully developed regions. Figure 13(*c*) shows the computational model accurately predicts the variation of centerline velocity along the channel for two Reynolds numbers. Figure 13(*d*) shows pressure drop across the channel is accurately predicted by both the computational model and empirical macrochannel pressure drop correlations that account for the inlet contraction, developing flow region, fully developed region, and outlet expansion. These findings prove that, for microchannel diameters of practical interest, the conventional Navier–Stokes equation accurately predicts single-phase liquid flow.

3.2 Effects of Microchannel Size and Shape on Heat Diffusion in Heat Sink. Because of the relative ease of fabricating rectangular microchannels, the vast majority of microchannel heat sink studies involve rectangular cross-sections. However, some investigators have also examined nonrectangular cross-sections such as triangular [91,92], trapezoidal [93,94], and diamond-shaped [95], pointing to the thermal benefits of individual shapes related to heat diffusion effects and bubble nucleation in sharp corners. Heat diffusion in the heat sink is responsible for an important thermal resistance between the device and the microchannel's wetted surface. Knowing this resistance allows the determination of the device temperature when the coolant temperature and heat transfer coefficient are known.

The one-dimensional fin analysis method is a convenient means to determining the heat diffusion resistance in a heat sink with rectangular microchannels provided the Biot number, based on half-width of the solid wall separating channels, is sufficiently small [96]. Recently, Kim and Mudawar [97,98] derived detailed one-dimensional analytical solutions for heat diffusion in heat sinks with rectangular, inverse trapezoidal, triangular, trapezoidal, diamond-shaped, and circular microchannels as illustrated in Fig. 14. When compared to detailed two-dimensional numerical models of the same cross-sections over a broad range of parameters, the analytical models proved very accurate. This proves the analytical models are very effective tools for the design and thermal resistance prediction of microchannel heat sinks. Detailed relations for the different geometries can be found in Refs. [97] and [98].

3.3 Mechanistic Definition of a Two-Phase Microchannel. One of the most controversial aspects of microchannel flow boiling is determining what constitutes a microchannel. From the standpoint of absolute hydraulic diameter scale, it would appear that "milli-channel" is a more appropriate designation since most two-phase microchannel heat sinks of practical interest possess diameters in the range of 0.1–0.6 mm rather than a micrometer [99]. However, a more rigorous definition of a microchannel is needed because the same channel may behave as a microchannel for certain fluids and operating conditions and macrochannel for others.

The boundary between microchannel and macrochannel two-phase flow is closely related to the ratio of bubble size to channel diameter, the larger the ratio, the more likely that the flow will behave as that of a microchannel. Bubble size can be determined by equating the liquid drag force on a bubble to the surface tension force that tends to preserve the bubble attachment to the wall [100].

$$C_D\left(\frac{\pi D_b^2}{4}\right)\frac{1}{2}\rho_f U^2 \sim \pi D_b \sigma \tag{1}$$

A channel tends to "confine" the flow when the diameter determined from Eq. (1) approaches the diameter of the channel. Therefore, the channel diameter corresponding to the transition from macrochannel to microchannel flow can be determined from the relation [68]

$$D_{\text{tran}} \leq D_b \tag{2}$$

Two-phase microchannel flow applications of practical interest possess modest laminar Reynolds numbers, generally greater than 50, for which the drag coefficient is given by [100]

$$C_D = \frac{24}{\text{Re}_{\text{tran}}}\left(1 + \frac{3}{160}\text{Re}_{\text{tran}}\right) \tag{3}$$

Combining Eqs. (1) to (3) and substituting $G = \rho_f U$ yield the following criterion for transitional channel diameter [68]

$$D_{\text{tran}} = \frac{160}{9}\frac{\left(\sigma\rho_f - 3\mu_f G\right)}{G^2} \tag{4}$$

Table 1 gives the values of D_{tran} for water and HFE 7100 based on Eq. (4). Use of a low surface tension fluid and/or increasing mass velocity is shown to enable smaller channels to behave as

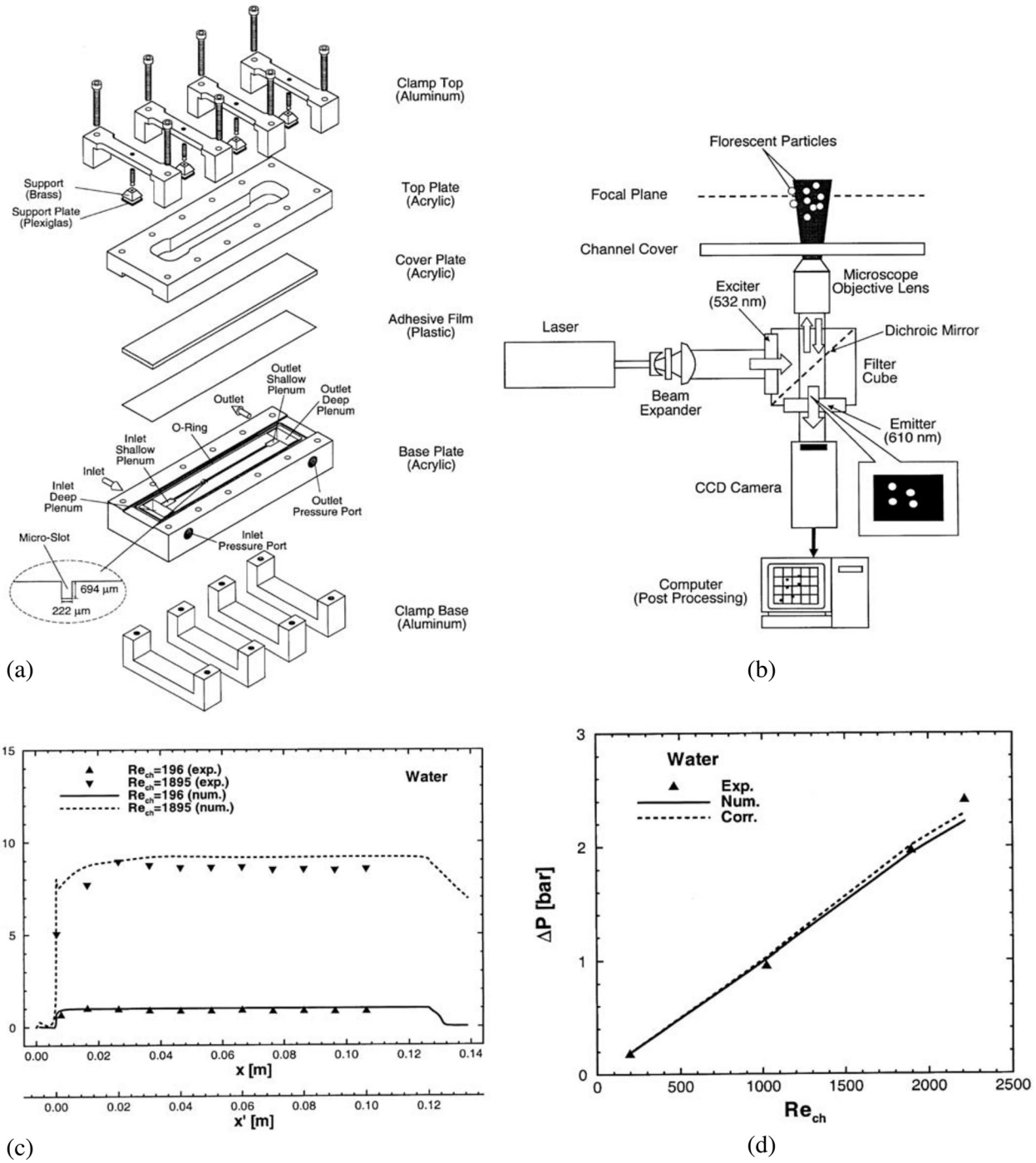

Fig. 13 (*a*) Schematic of single microslot module used for micro-PIV measurement of single-phase water flow; (*b*) micro-PIV system; (*c*) comparison of measured and numerically predicted centerline velocity along flow direction; and (*d*) comparison of measured pressure drop and predictions based on numerical analysis and macrochannel correlations [90].

macrochannels. For example, flow boiling of HFE 7100 with $G < 2000\,\mathrm{kg/m^2s}$ in a 0.086 mm channel can be categorized as macrochannel flow, whereas that of water with $G > 500\,\mathrm{kg/m^2s}$ in a 3.99 mm channel would behave as microchannel flow!

Note that Eq. (4) can also be expressed as a Weber number criterion for confinement

$$\mathrm{We}_{\mathrm{tran}} = \frac{160}{9}\frac{1}{\left(1+\dfrac{160}{3\mathrm{Re}_{\mathrm{tran}}}\right)} \tag{5}$$

which can be further approximated as $\mathrm{We}_{\mathrm{tran}} = 160/9$ for high mass velocities.

3.4 Incipient Boiling. Small size and noncircular cross-section pose two major challenges to predicting the inception of boiling in a microchannel using macrochannel boiling incipience models (e.g., Refs. [101] and [102]). Qu and Mudawar [103,104] explored the impact of both channel shape and size on bubble departure criteria and developed a mechanistic model to predict the incipient boiling heat flux, q''_i. Their model is based on two key criteria, one is hydrodynamic and the second thermal. The hydrodynamic criterion requires that bubble departure can occur only when the drag force exerted by the liquid on the bubble exceed the surface tension force responsible for bubble attachment to the channel wall. The thermal criterion requires that the bubble will

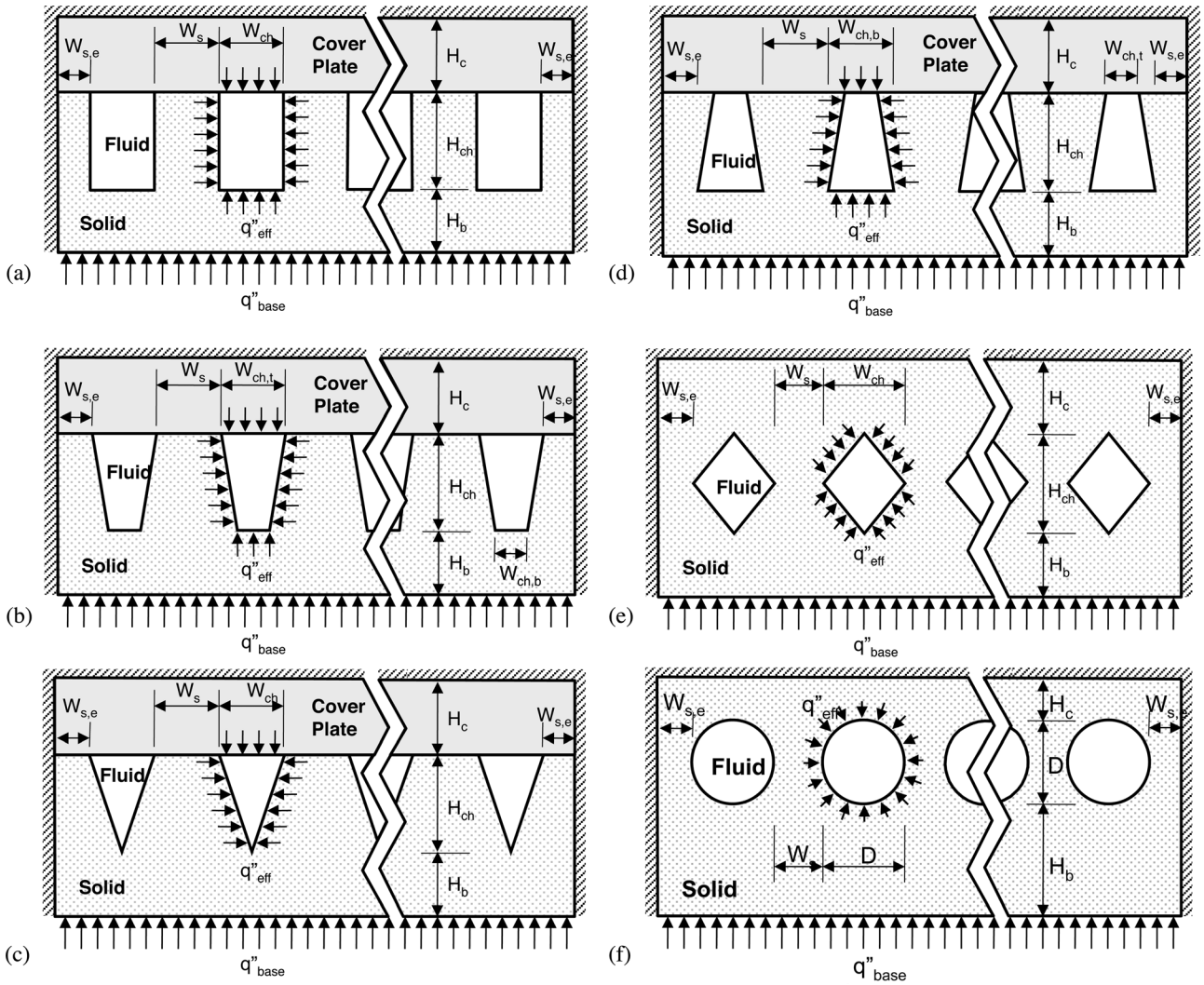

Fig. 14 Schematic diagrams of microchannel heat sinks with (*a*) rectangular, (*b*) inverse-trapezoidal, (*c*) triangular, (*d*) trapezoidal, (*e*) diamond-shaped, and (*f*) circular cross-sections. (Adapted from Kim and Mudawar [97,98])

grow and detach only when the lowest temperature along its interface exceed the saturation temperature. Since boiling commences at the channel outlet, both the hydrodynamic and thermal criteria must be examined at the outlet, which requires the determination of the liquid velocity and temperature distributions at that location just prior to initiation of boiling.

Unlike the simple model of force balance on a bubble presented in Sec. 3.3, the hydrodynamic criterion used in the boiling incipience model included the detailed shape of the departing bubble. A previous model of bubble shape and forces by Al-Hayes and Winterton [105] was modified to account for bubble growth in a rectangular microchannel. Bubble growth was first examined for three possible regions of the channel closest to the heated bottom wall: the bottom wall itself, sidewalls, and bottom corner, as illustrated in Fig. 15(*a*). To determine the radius of a departing bubble, r_b, the bubble is treated as a truncated sphere that maintains contact angles with the wall equal to the equilibrium contact angle θ_0. The bubble can depart when the liquid drag force, F_D, just exceed the surface tension force, F_s.

The drag force is assumed proportional to the product of projected area of the bubble facing the flow and the dynamic pressure of the liquid [106]

$$F_D = C_D \frac{1}{2} \rho_f u_e^2 A_p \tag{6}$$

TABLE 1 Fluid properties and hydraulic diameters corresponding to transition from macrochannel to microchannel flow for water and HFE 7100 at one bar based on Eq. (4)

Fluid	T_{sat} (°C)	ρ_f (kg/m^3)	μ_f (kg/m s)	σ (mN/m)	G (kg/m^{2}s)	D_{tran} (mm)
Water	99.6	959	2.83×10^{-4}	59	500	3.99
					1000	0.99
					2000	0.24
HFE 7100	59.6	1373	3.57×10^{-4}	15.7	500	1.49
					1000	0.36
					2000	0.086

where C_D, A_p, and u_e are the drag coefficient, projected area of the bubble, and velocity at a point e halfway to the bubble tip, respectively. The projected area can be determined geometrically in terms of r_b and θ_o and has different formulations for the bottom and sidewalls as compared to the corners. Furthermore, the corner expression for A_p is different for the range of $0 \le \theta_0 \le \pi/4$ compared to that for $\pi/4 \le \theta_0 \le \pi/2$.

The drag coefficient C_D in Eq. (6) can be expressed as a function of the bubble Reynolds number $\mathrm{Re}_b = \rho_f u_e(2r_b)/\mu_f$ [106], and the surface tension force is evaluated as

$$F_s = C_s \frac{1}{4}\sigma P_c(\cos\theta_r - \cos\theta_a) \tag{7}$$

where P_c, θ_r, and θ_a are the length of the contact line, receding contact angle, and advancing contact angle, respectively.

Like the projected area, different geometrical relations for P_c are used for the bottom wall and sidewalls compared to the corners; there relations are expressed in terms of the modified contact angles at the bubble's upstream and downstream stagnation points, θ_a and θ_r, respectively, as illustrated in Fig. 15(*b*).

Combining the relations for A_p and P_c with Eqs. (6) and (7) yield the following relations:

$$\text{Bottomwall and sidewalls}: u_e^2 r_b = \frac{C_s}{C_d}\frac{\sigma}{\rho_f}\frac{\pi \sin\theta_0(\cos\theta_r - \cos\theta_a)}{\pi - \theta_0 + \cos\theta_0 \sin\theta_0} \tag{8}$$

$$\text{Corners}: u_e^2 r_b = \begin{cases} \dfrac{C_s}{C_d}\dfrac{\sigma}{\rho_f}\dfrac{2\pi \sin\theta_0(\cos\theta_r - \cos\theta_a)}{\pi - 2\theta_0 + 2\cos\theta_0 \sin\theta_0} & \text{for } 0 \le \theta_0 \le \dfrac{\pi}{4} \\ \dfrac{C_s}{C_d}\dfrac{\sigma}{\rho_f}\dfrac{2\left[\pi - \arccos\left(\frac{\cos\theta_0}{\sin\theta_0}\right)\right]\sin\theta_0(\cos\theta_r - \cos\theta_a)}{\frac{3\pi}{4} - \theta_0 + \cos\theta_0(\cos\theta_0 + \sin\theta_0)} & \text{for } \dfrac{\pi}{4} \le \theta_0 \le \dfrac{\pi}{2} \end{cases} \tag{9}$$

To determine u_e in the above equations, fully developed single-phase laminar liquid flow is assumed just upstream of the bubble. Given the velocity field, Fig. 15(*c*), Eqs. (8) and (9) can be used to determine the radius of a departing bubble, r_b, from which the geometry of the bubble can be easily specified. These relations show r_b decreases with increasing liquid velocity and that corner bubbles are substantially larger than those at the bottom wall or sidewalls.

The second criterion of the incipience model requires that entire bubble interface be superheated before a bubble can depart; i.e., the lowest temperature along the bubble's interface must exceed the saturation temperature. This requires determining the detailed temperature distribution around the bubble to locate the lowest temperature along the interface. This in turn requires to determining the liquid temperature distribution at the exit and geometry of the departing bubble. The temperature distribution in the liquid, Fig. 15(*d*), can be determined by solving the energy equation assuming fully developed single-phase laminar liquid flow. To determine the incipience condition, the heat flux is increased until a bubble is found at the exit that satisfies the superheat criterion at the exit.

Notice in the temperature plot in Fig. 15(*d*) that the wall temperature is highest and temperature gradient smallest at the corner. This means a bubble near the corner region is easier to nucleate than bubbles elsewhere along the microchannel walls. However, the model shows the first bubble to nucleate is located at the bottom wall close to, but not at, the channel corner. The reason why the corner bubble does not nucleate first is that the corner bubble is larger and, therefore, penetrates deeper into the cooler liquid than a smaller bubble forming on the bottom wall close to the corner. Figure 15(*e*) shows the measured incipient boiling heat flux, q_i'', increases with increasing inlet liquid velocity, u_{in}, and decreasing inlet temperature, T_{in}. Also, shown in Fig. 15(*e*) are predictions based on the incipience model. Two values of equilibrium contact angle, 30 deg and 80 deg, are assumed because the actual contact angle falls within this range for water on a copper surface. The differences between predictions *using* the two values are relatively small, providing a good agreement with the incipient boiling heat flux data.

3.5 How Useful Are Microchannel Two-Phase Flow Regime Maps? Knowledge of flow regime and flow regime transitions is essential to the development of reliable predictive tools for pressure drop and heat transfer in two-phase microchannel heat sinks, and small microchannel size can have a profound effect on flow regime development [107,108]. As pointed out by Hosler [109], knowing which two-phase flow regime prevails in a microchannel is analogous to knowing whether a single-phase flow is laminar or turbulent.

Adiabatic two-phase flow regimes in rectangular mini/microchannels have been discussed in several recent studies. Examples include works by Wambsganss et al. [110], Ali and Kawaji [111], Mishima et al. [112], Fujita et al. [113], and Xu et al. [114]. What emerge from all these studies are flow regimes similar to those found in macrochannels but with significant variations, such as the absence of churn flow for very small hydraulic diameters [111]. Additionally, most investigators conclude that, while macrochannel flow regime maps do capture overall qualitative trends, they cannot be relied upon for quantitative predictions.

Figure 16(*a*) shows a flow module that was constructed by Qu et al. [115] to investigate adiabatic two-phase flow regimes in a horizontal 0.406 mm deep, 2.032 mm wide, and 12 cm long microchannel. Figure 16(*b*) depicts the construction of a mixer containing a 40 μm porous tube, which was used to bubble nitrogen gas from the core into a water stream passing through the annulus between the porous tube and housing. Figure 16(*c*) depicts the five flow regimes they captured: slug, annular, bubbly/slug, liquid/slug and liquid/annular. Figure 16(*d*) depicts these flow regimes and their transition boundaries in a flow pattern map utilizing the superficial velocities of nitrogen and water as coordinates. At low values of j_f, the dominant regimes are slug or bubbly/slug for low j_g and annular for high j_g. For high values of j_f, the flow transitions from liquid/slug to liquid/annular increase with increasing j_g. Figures 16(*e*) and 16(*f*) compare their flow regime map to popular adiabatic macrochannel maps by Mandhane et al. [116] and Taitel and Duckler [117], respectively. These figures show significant discrepancy with the microchannel data of Qu et al., a conclusion agreed upon by many of those who investigated microchannel flow regimes as discussed earlier.

These discrepancies can be attributed to several factors, including the relatively strong influence of surface tension and negligible gravitational effects in microchannel flow. In addition, low flow rates in microchannels often produce laminar liquid and gas flows, a combination less commonly encountered in macrochannels. Flow regime determination is even more complicated during

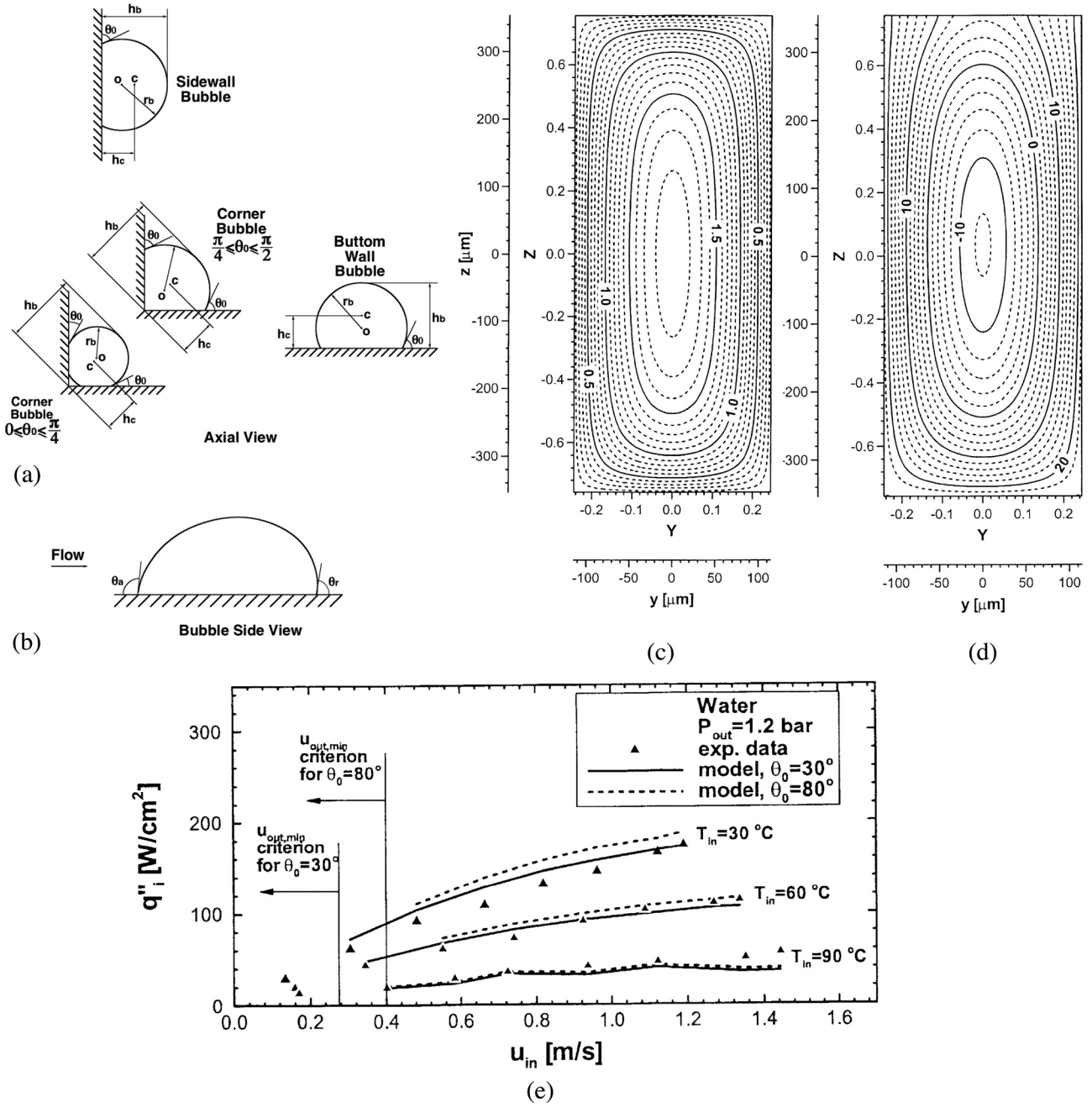

Fig. 15 (*a*) **Appearance of departing bubbles along microchannel cross-section, (*b*) stream-wise deformation of bubble. Dimensionless (*c*) liquid velocity, (*d*) liquid temperature contours at microchannel exit; and (*e*) comparison of incipience model predictions with experimental data for water. (Adapted from Qu and Mudawar [103]).**

flow boiling in microchannels, where interfacial interactions between the vapor and liquid can have profound influences on flow regime development. The situation is further complicated with practical microchannel heat sinks containing a large number of parallel channels, where two-phase flow is subject to instabilities caused by interactions between channels and between the heat sink as a whole and the rest of the cooling loop.

These facts bring into question, the usefulness of microchannel flow regime maps. To answer this question, one must first realize the fundamental weaknesses of such maps, even for macrochannels. First, using superficial velocities as coordinates for these maps assume that these velocities alone dictate flow regime. This is obviously a very simplistic and erroneous assumption. The second weakness is the fact that flow regime transitions are dominated by physical mechanisms and corresponding dimensionless groups that vary greatly from one transition boundary to another. Because it is virtually impossible to present transitions corresponding to a large number of dimensionless groups in a two-dimensional map, the accuracy of the entire map approach must be questioned. It is, therefore, more appropriate to implement a series physical transition models to determine the prevalent flow regime. This also requires the use of proper dimensionless groups in the transition models. As indicate by Qu et al. [115], those should include at a minimum

$$\text{Phase Reynolds numbers: } \mathrm{Re}_f = \frac{\rho_f j_f D_h}{\mu_f} \text{ and } \mathrm{Re}_g = \frac{\rho_g j_g D_h}{\mu_g} \tag{10}$$

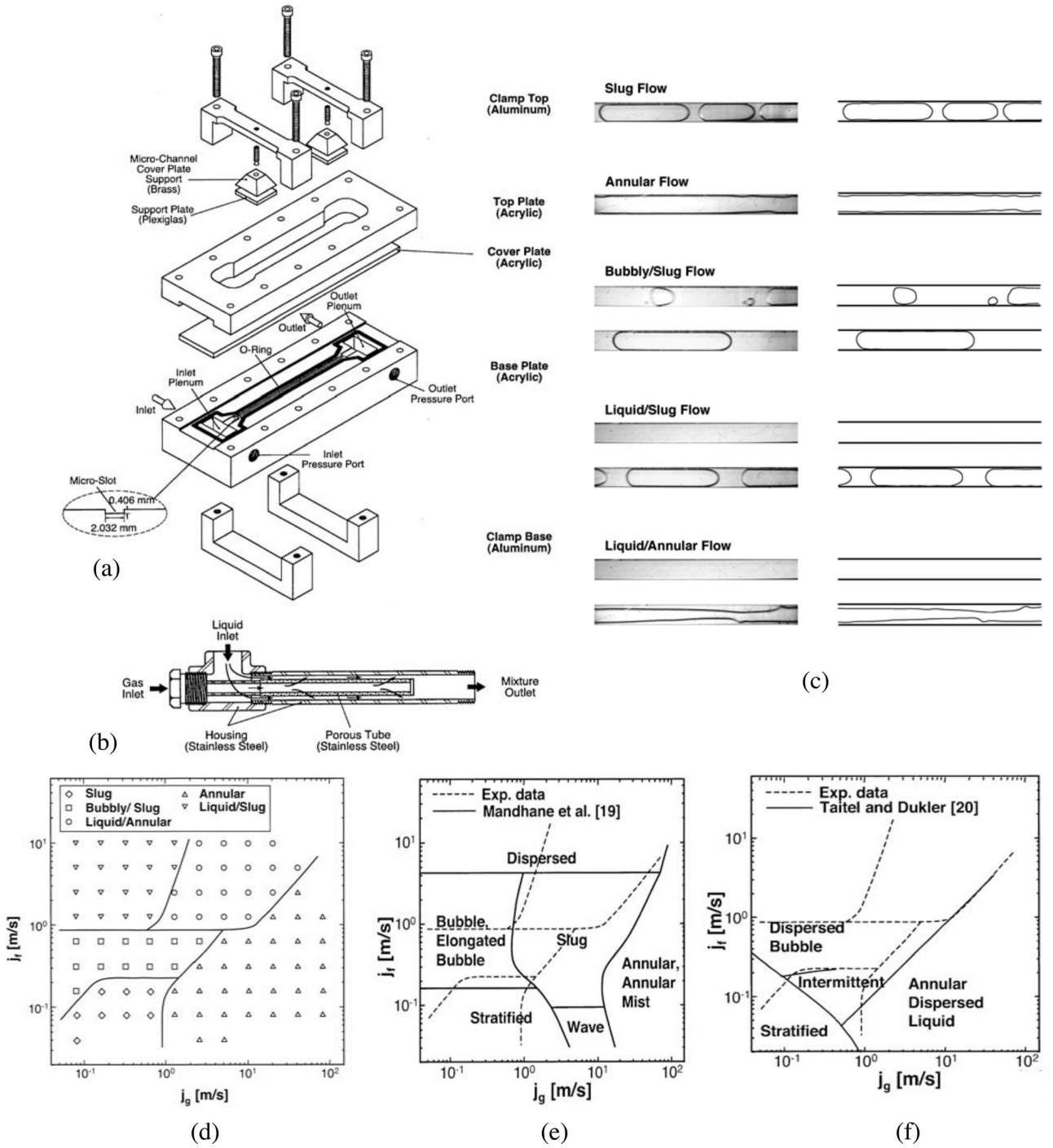

Fig. 16 (*a*) **Test module for adiabatic microchannel two-phase flow regimes study.** (*b*) **Construction of nitrogen-water mixer.** (*c*) **Photographs and schematics of two-phase flow regimes.** (*d*) **Two-phase regime map.** (*e*) **Comparison of flow regime map with macro-channel map of Mandhane et al. [116].** (*f*) **Comparison of flow regime map with macrochannel map of Taitel and Dukler [117]. (Adapted from Qu et al. [115]).**

$$\text{Phase Weber numbers: } \mathrm{We}_f = \frac{\rho_f j_f^2 D_h}{\sigma} \text{ and } \mathrm{We}_g = \frac{\rho_g j_g^2 D_h}{\sigma} \quad (11)$$

$$\text{Phase Froude numbers: } \mathrm{Fr}_f = \frac{j_f^2}{g_e D_h} \text{ and } \mathrm{Fr}_g = \frac{j_g^2}{g_e D_h} \quad (12)$$

$$\text{Capillary number: } \mathrm{Ca} = \frac{\mu_f j_f}{\sigma} \quad (13)$$

$$\text{Confinement number: } \mathrm{Co} = \frac{\sqrt{\frac{\sigma}{g_e(\rho_f - \rho_g)}}}{D_h} \quad (14)$$

$$\text{and superficial slipratio: } S = \frac{j_g}{j_f} \quad (15)$$

It should be noted, however, that groups that include g_e have a weaker impact on microchannel flows than macro, given the relatively higher inertial and surface tension forces in small channels.

3.6 Two-Phase Flow Instabilities. Hydrodynamic instabilities are common to flow boiling systems [118,119]. Two-phase mixture compressibility and use of multiple parallel flow channels render such instabilities a key concern with two-phase microchannel heat sinks. Two types of flow instabilities have been identified in such heat sinks [120]: (1) severe pressure drop oscillation and (2) mild parallel channel instability.

The severe pressure oscillation occurs in the absence of a flow resistance, such as a throttling valve, upstream of the heat sink, where vapor generation in the channels could communicate with the compressible volume in the flow loop upstream of the heat sink. As shown in Fig. 17(*a*), this form of instability is manifest by the boiling boundary between the single-phase liquid and two-phase mixture in all channels of the heat sink oscillating back and forth in unison between the inlet and the outlet, resulting in appreciable pressure oscillations. At high heat fluxes, the oscillation can be so severe that vapor could enter the inlet plenum. This form of instability could be explained as follows. After boiling commences inside the heat sink, vapor production increases flow resistance in the channels. In the presence of a relatively large compressible volume in the flow loop upstream of the heat sink, the increased flow resistance reduces the coolant flow rate into the heat sink, which in turn escalates vapor production in the channels. The reduction in flow rate is confined to the heat sink because the flow loop is designed to deliver a constant flow rate. Increased flow resistance in the channels now begins to raise the heat sink's upstream pressure. The upstream pressure continues to rise until it is able to expel the vapor completely out of the channels. With liquid now flowing through the channels, both the flow resistance and upstream pressure decrease until vapor is generated once more in the channels, and a new period of oscillation is initiated. As discussed in a later section, this type of instability is highly undesirable and must be avoided not only due to the large flow and pressure oscillations involved but because it may also induce pre-mature CHF. Fortunately, the severe pressure drop oscillation can be virtually eliminated by throttling the flow immediately upstream of the test module.

With adequate upstream flow throttling, only the second mild parallel instability is encountered [120]. As shown in Fig. 17(*b*), this instability takes the form of random fluctuations of the boiling boundary between microchannels. The spatial amplitude of fluctuation of the boiling boundary is much smaller than with the severe pressure drop oscillation. The mild parallel instability is the result of a density wave oscillation within each channel and feedback interaction between channels. It is mild enough that its occurrence does not compromise the heat sink's cooling performance.

3.7 Prediction of Two-Phase Pressure Drop. Despite decades of efforts to arrive at a universal approach to predicting pressure drop in two-phase microchannel flow, drastic differences in pressure drop predictions often confound researchers despite the use of seemingly similar approaches in tackling two-phase pressure drop components. A simple explanation for these differences is the existence of many components of pressure drop, as depicted in Fig. 18. A complete pressure drop model must be able to tackle 11 different components, encompassing the inlet contraction, single-phase liquid region, subcooled two-phase region, saturated

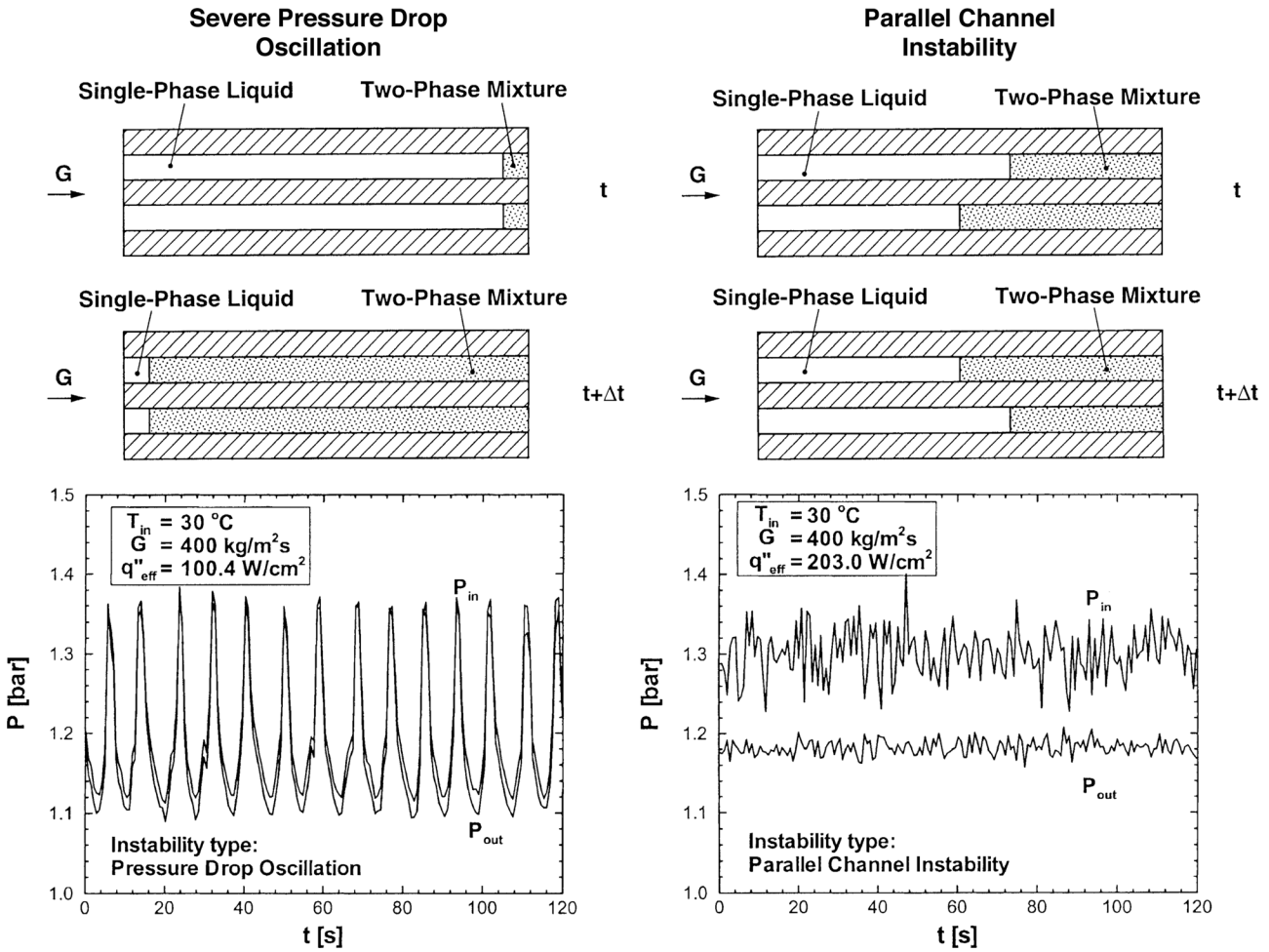

Fig. 17 Top view depictions of two neighboring microchannels and temporal records of inlet and outlet pressures during (*a*) severe pressure drop oscillation and (*b*) mild parallel channel instability. (Adapted from Qu and Mudawar [120])

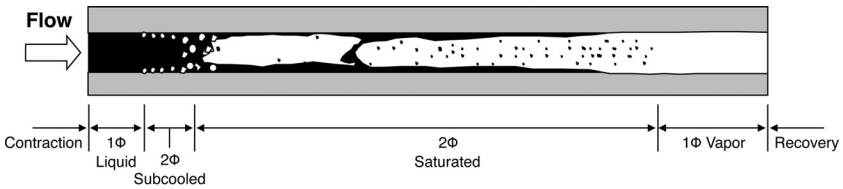

1. Inlet contraction
2. Developing laminar single-phase liquid region
3. Developing turbulent single-phase liquid region
4. Fully-developed laminar single-phase liquid region
5. Fully-developed turbulent single-phase liquid region
6. Subcooled two-phase region
7. Saturated two-phase region friction
8. Saturated two-phase region acceleration
9. Laminar single-phase vapor region
10. Turbulent single-phase vapor region
11. Outlet pressure recovery

Fig. 18 Components of a complete two-phase microchannel flow pressure drop model

two-phase region, single-phase vapor region, and outlet recovery, with pressure drop in some regions consisting of different subcomponents. And while the two-phase regions generally contribute the largest percentage of total pressure drop, accurate prediction of every one of the components listed in Fig. 18 is essential to arriving at a good overall pressure drop prediction. For example, poor prediction of the *extent* of the single-phase regions can result in large errors in predicting the extent of the two-phase regions as well, which compromises the accuracy of the overall pressure drop prediction regardless of the accuracy of the two-phase models used. Given the large number of subregions and availability of multiple competing models for the individual subregions, a conservative (and by means conclusive) estimate by the author leads to 31.6×10^6 possible predictions of pressure drop for a given set of operating conditions!

Another reason for poor predictions of pressure drop (and heat transfer coefficient) is the relative poor quality of many microchannel flow databases that two-phase models and correlations are built upon. For a database to contribute effectively to the development of an accurate two-phase microchannel pressure drop model or correlation, it must satisfy several important criteria, including (1) a sufficiently large number of data points, (2) data for fluids with drastically different thermophysical properties (e.g., fluorochemical dielectric liquid coolants and refrigerants versus water), (3) identification of the extent of all dominant flow regimes through flow visualization, (4) careful distinction of the subcooled and saturated boiling regions (rather than attempting to lump the two together), (5) careful assessment of measurement uncertainty (this is especially the case when isolating heat loss from measurements of heat transfer coefficient and CHF), and (6) reliance on dimensionless groups that capture dominant physical interactions for characterizing the individual flow regions.

Prediction of pressure drop for the single-phase liquid region must first include the overall extent of the single-phase region, which can be determined from a boiling incipience model as discussed in Sec. 3.4. This must be followed by determination of the

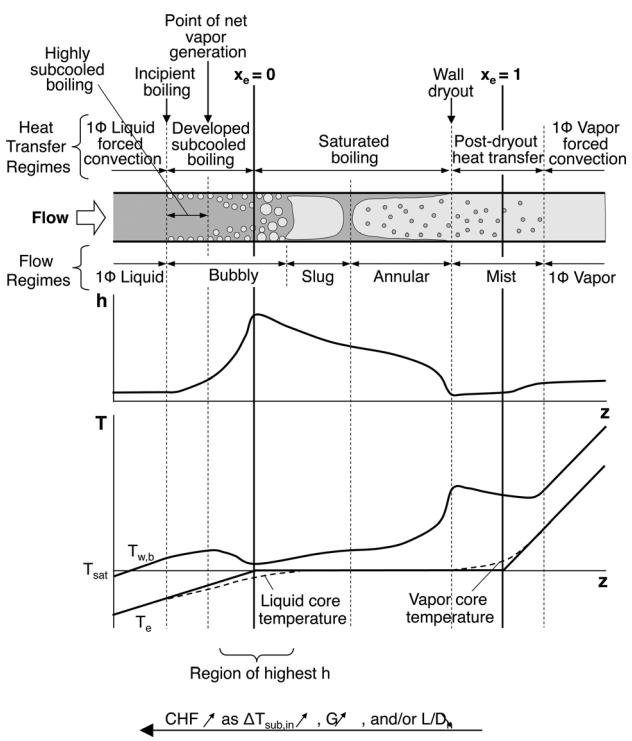

Fig. 19 Flow regimes, heat transfer regimes, and variations of wall temperature and convective heat transfer coefficient along microchannel flow

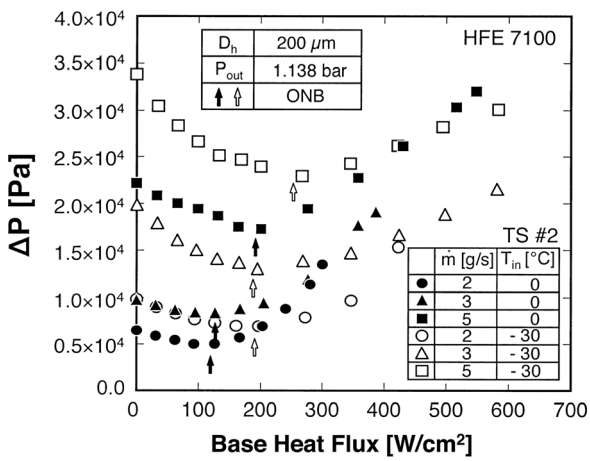

Fig. 20 Variation of subcooled boiling pressure drop with base heat flux. (Adapted from Lee and Mudawar [67])

extent of the developing and fully developed portions of the single-phase liquid region using a relation such that of Shah and London [121].

$$L_{sp,d} = (0.06 + 0.07\beta - 0.04\beta^2)\mathrm{Re}_{in}D_F \tag{16}$$

where β is the microchannel's aspect ratio ($0 < \beta < 1$ when used in Eq. (16)). Pressure drop across the two liquid regions can also be predicted with good accuracy using correlations by Shah and London. A similar approach may be used to predict pressure drop across the downstream single-phase vapor region.

Subcooled flow boiling occurs when bubbles begin to form along the microchannel walls, but upstream of the location where $x_e = 0$, as illustrated in Fig. 19. The subcooled boiling region is comprised of two zones, a *highly subcooled zone*, whose upstream edge corresponds to the onset of boiling, and a *developed subcooled zone*. Within the highly subcooled zone, bubbles are able to form but show minor growth while still attached to the wall. On the other hand, bubbles in the developed subcooled zone can detach into the liquid flow where they condense slightly but are able to endure and even coalesce with one another.

Because of strong departure from thermodynamic equilibrium, predicting pressure drop for the subcooled boiling region is quite illusive. As subcooled liquid heat ups along the microchannel, its viscosity decreases. Increasing the wall heat flux causes further reduction in liquid viscosity. Therefore, pressure drop associated with pure liquid flow decreases with increasing wall heat flux. The trend changes significantly when bubbles begins to form. Here, increasing wall heat flux increases both the two-phase frictional and accelerational gradients of pressure drop. Pressure drop, therefore, begins to increase with increasing heat flux. This trend is depicted in Fig. 20. Lee [122] developed a theoretical model to predict the subcooled boiling pressure drop.

There are three different approaches to predicting pressure drop across the saturated vapor region: (1) homogeneous equilibrium model (HEM), (2) separated flow models (SFMs), and (3) theoretical models. The study by Qu and Mudawar [120] provides a theoretical basis for models of saturated pressure drop and heat transfer in microchannels. These models are based on the use of control volumes for the liquid and combined flow, coupled with an expression for interfacial shear stress that accounts for interfacial phase change, and a model for droplet entrainment and deposition.

HEM is by far the simplest of pressure drop models and is based on the assumptions of both uniform and equal phase velocities. Accounting for property variations, pressure drop can be determined by integrating the following relation for pressure gradient [13,15]

$$-\left(\frac{dP}{dz}\right) = \frac{\left\{1 + \frac{G^2 v_{fg}}{h_{fg}}\left[x v_g + (1-x)v_f\right]\right\}\frac{\tau_F \mathrm{P}_F}{A} + G v_{fg}\left(\frac{q''_{\mathrm{eff}}\mathrm{P}_H}{Ah_{fg}}\right)}{\left\{1 + \frac{G^2 v_{fg}}{h_{fg}}\left[x v_g + (1-x)v_f\right]\right\} + G^2\left[x\frac{dv_g}{dP} + (1-x)\frac{dv_f}{dP}\right] - \frac{G^2 v_{fg}}{h_{fg}}\left[x\frac{dh_g}{dP} + (1-x)\frac{dh_f}{dP}\right]} \tag{17}$$

which couples the momentum and energy equations for homogeneous two-phase flow. A key unknown in the above equation is the wall shear stress, τ_F, which can be determined from the relation

$$\tau_F = \frac{1}{2} f_{tp}\bar{\rho}u^2 = \frac{1}{2} f_{tp}\left(v_f + x v_{fg}\right)G^2 \tag{18}$$

Using Eq. (18), the wall shear stress can be expressed in terms of either a constant empirical two-phase friction factor, f_{tp}, or the "liquid-only" single-phase friction factor, f_{fo}, using an appropriate model for two-phase mixture viscosity, $\bar{\mu}$ [123–127].

$$f_{tp} = f_{fo}\left(\frac{\bar{\mu}}{\mu_f}\right)^n = \frac{C}{\left(\frac{GD_F}{\mu_f}\right)^n}\left(\frac{\bar{\mu}}{\mu_f}\right)^n \tag{19}$$

where the constants C and n depend on whether the equivalent single-phase flow is laminar or turbulent.

One of the key advantages of HEM is the ease with which both compressibility and flashing effects may be ascertained. The former accounts for specific volume variations with pressure, and the latter latent heat variations with pressure; both effects are included in the denominator of Eq. (17). Notice also that by expressing the denominator of Eq. (17) as $(1 - M^2)$, where M is the two-phase Mach number, HEM can be effective at predicting choking in the microchannel.

Separated pressure drop models are fundamentally different from HEM in that they allow for differences between the phase velocities. However, their ability to more realistically capture two-phase flow behavior is compromised by an inability to analytically relate thermodynamic equilibrium quality, x_e, which is easily determined from mass and energy conservation, to the more elusive void fraction, α. This why other models are needed to relate these two important parameters, such as the Zivi relation [128]

$$\alpha = \left[1 + \left(\frac{1-x_e}{x_e}\right)\left(\frac{v_f}{v_g}\right)^{2/3}\right]^{-1} \tag{20}$$

in order to predict two-phase pressure drop.

The SFMs involve determining the accelerational and frictional components of pressure drop independently. Using the Zivi relation, the accelerational component can be determined by integrating the expression

$$-\left(\frac{dP}{dz}\right)_{tp,A} = G^2\frac{dx_e}{dz}\left[\left(\frac{2v_g x_e}{\alpha} - \frac{2v_f(1-x_e)}{(1-\alpha)}\right) + \frac{d\alpha}{dx_e}\left(-\frac{v_g x_e^2}{\alpha^2} + \frac{v_f(1-x_e)^2}{(1-\alpha)^2}\right)\right] \tag{21}$$

Most recently published works for predicting pressure drop in microchannels employ SFMs based on the Lockhart–Martinelli method [129]. Using this method, the friction factor for each phase is based on the actual flow rate of the individual phase to determine the Lockhart–Martinelli parameter, X.

$$X = \left[\frac{-(dP/dz)_{F_f}}{-(dP/dz)_{F_g}}\right]^{0.5} \tag{22}$$

In recent years, several correlations that are based on the Lockhart–Martinelli method (e.g., Refs. [61], [64], and [130])

have been recommended for predicting the two-phase frictional pressure drop in microchannels. Most are very similar in formulation except for specific relations that are adopted to account for small channel size. For example, the correlation of Lee and Mudawar [64] modifies the constant C in the original Lockhart–Martinelli method

$$\Delta P_{tp,F} = \frac{2G^2 L_{tp}}{D_F x_{e,\text{out}}} \int_{x_{e,in}}^{x_{e,\text{out}}} f_f (1 - x_e) \upsilon_f \left(1 + \frac{C}{X} + \frac{1}{X^2}\right) dx_e \tag{23}$$

with separate functions of the liquid-only Reynolds number and Weber number, segregated by dominant two-phase flow patterns. Figure 21 illustrates the effectiveness of this correlation at predicting saturated boiling pressure drop in microchannels for fluids with drastically different thermophysical properties.

Finally, contraction pressure drop and expansion pressure recovery can be determined from correlations that account for both area changes and microchannel shape [131,132].

3.8 Prediction of Two-Phase Heat Transfer Coefficient. Heat transfer coefficient in the fully developed single-phase liquid region can be predicted quite accurately according to relations by Shah and London [121], which account for aspect ratio of rectangular channels. The same relations may be applied to the downstream fully developed single-phase vapor region. However, additional tools are required to tackle the upstream developing liquid region. This can be accomplished with the aid of correlations by Copeland [133] and Al-Arabi [134].

Lee and Mudawar [67] examined several macrochannel subcooled boiling correlations and found them unsuitable for microchannel flow. They developed the following correlation:

$$\frac{h_{sc}}{h_{sp}} = 90.0 \left(\frac{q''_{\text{base}}}{G\, h_{fg}}\right)^{0.9} \left(\frac{c_{pf}\, \Delta T_{\text{sub},in}}{h_{fg}}\right)^{-0.98} \text{We}^{*\,0.15}\, \beta^{0.42} \tag{24}$$

where

$$\text{We}^* = \frac{G^2 D_h}{\left(\rho_f - \rho_g\right)\sigma} \text{and} \beta = \frac{W_{ch}}{H_{ch}} \tag{25}$$

which was based on a large database for subcooled flow boiling of HFE 7100 in microchannels. Equation (24) is expressed as a ratio of the two-phase heat transfer coefficient to that for single-phase liquid flow at the same flow rate, and q''_{base} is the base heat flux for the microchannel heat sink.

Several heat transfer correlations have been recommended for the saturated boiling region. Since most were developed for uniform circumferential heating, while most microchannel heat sinks involve rectangular channels with three-sided heating, these correlations must be modified according to the relation [64]

$$h_{\text{sat}} = h_{\text{sat,cor}} \frac{\text{Nu}_3}{\text{Nu}_4} \tag{26}$$

where $h_{sat,cor}$ is the value predicted from the correlation, and Nu_3 and Nu_4 are the single-phase Nusselt numbers for fullydeveloped laminar flow with three-sided and four-sided wall heating, respectively [121].

$$\text{Nu}_3 = 8.235\left(1 - 1.833\,\beta + 3.767\,\beta^2 - 5.814\,\beta^3 + 5.361\,\beta^4 - 2.0\,\beta^5\right) \tag{27}$$

and

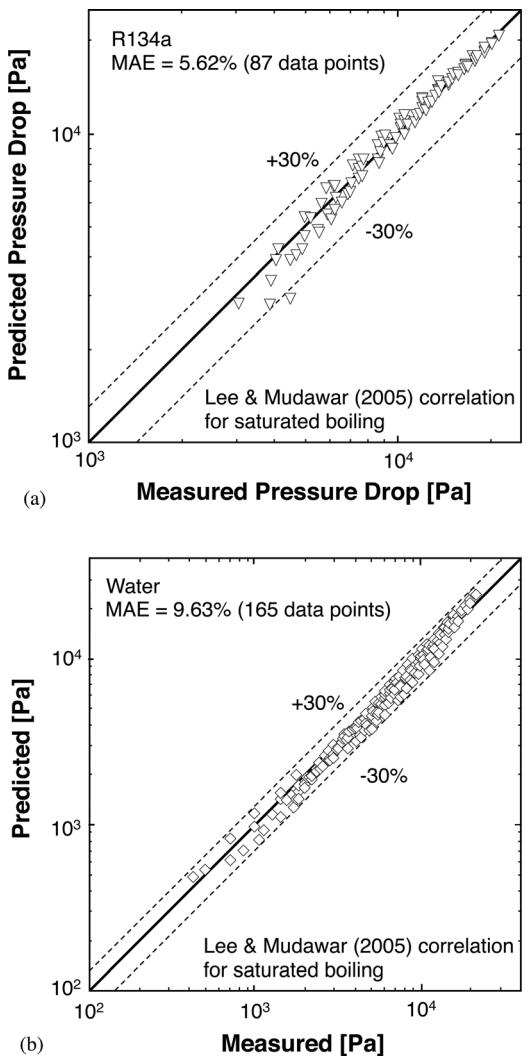

Fig. 21 Comparison of predictions of Lee and Mudawar correlation [64] for saturated boiling pressure drop with (*a*) Lee and Mudawar's R134a data [64] and (*b*) Qu and Mudawar'swater data [120]. (Adapted from Lee and Mudawar [64])

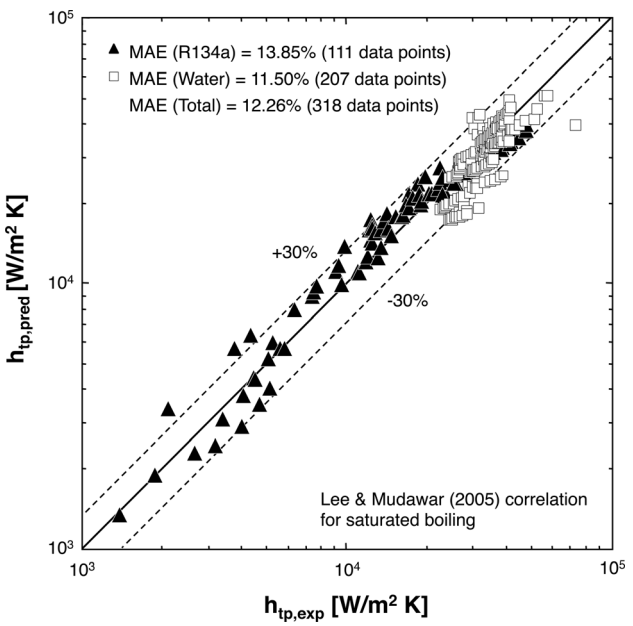

Fig. 22 Comparison of predictions of Lee and Mudawar correlation [65] for saturated boiling heat transfer coefficient with (*a*) Lee and Mudawar's R134a data [65] and (*b*) Qu and Mudawar's water data [62]. (Adapted from Lee and Mudawar [65])

$$\mathrm{Nu}_4 = 8.235\left(1 - 2.042\beta + 3.085\beta^2 - 2.477\beta^3 + 1.058\beta^4 - 0.186\beta^5\right) \tag{28}$$

Some of the correlations that have been used to predict the saturated boiling heat transfer coefficient, such as those of Chen [135], Shah [136], Gungor and Winterton [137], Kandlikar [138], Liu and Winterton [139], and Steiner and Taborek [140] are generally intended for macrochannel flow. Others, such as those of Lazarek and Black [141], Tran et al. [142], Lee and Lee [143], Yu et al. [144], Warrier et al. [145], and Lee and Mudawar [65], were developed specifically for small channels. The Lee and Mudawar correlation is presented in terms of the Lockhart–Martinelli parameter, the single-phase heat transfer coefficients for fully developed liquid and vapor flows, and the boiling number. This correlation is divided into three ranges of thermodynamic equilibrium quality to more effectively capture the influence of dominant flow regimes within each range.

$$h_{\mathrm{sat}} = \begin{cases} 3.856X^{0.267}h_{sp,f} & \text{for } 0 \le x_e < 0.05 \\ 436.48\left(\dfrac{q''_{ch}}{\mathrm{Gh}_{fg}}\right)^{0.522}\mathrm{We}_{fo}^{0.351}X^{0.665}h_{sp,f} & \text{for } 0.05 \le x_e < 0.55 \\ \mathrm{Max}\left\{\left(108.6X^{1.665}h_{sp,g}\right), h_{sp,g}\right\} & \text{for } 0.55 \le x_e \le 1.0 \end{cases} \tag{29}$$

where

$$h_{sp,g} = \begin{cases} \dfrac{\mathrm{Nu}_3 k_g}{D_h} & \text{for laminar vapor flow} \\ 0.023\mathrm{Re}_g^{0.8}\mathrm{Pr}_g^{0.4}k_g/D_h & \text{for turbulent vapor flow} \end{cases} \tag{30}$$

Figure 22 shows this correlation is highly effective at predicting the heat transfer coefficient for saturated boiling in microchannels for fluids with drastically different thermophysical properties.

3.9 Prediction of Critical Heat Flux. CHF correlations are available mostly for single channels and not recommended for microchannel heat sinks because of the strong influence of parallel channel interactions. Nonetheless, single-channel correlations provide a useful foundation for the formulation of CHF correlations for heat sinks.

For conventional macrochannels, Katto and Ohno's CHF correlation [146] are widely used and cover a wide range of parameters. Hall and Mudawar correlations [147,148] are based on the Purdue University Boiling and Two-Phase Flow Laboratory CHF database, which contains the largest database for subcooled and saturated CHF in the literature. The Hall and Mudawar correlations were validated over a broad range of pressures (from atmospheric to near the critical point) and mass velocities (300-30,000 kg/s.m^2). An earlier correlation by Hall and Mudawar [29], which is based on Mudawar and Bowers' ultra-high CHF database [27] (as high as 27,600 W/cm^2) in small diameter tubes, is better suited for microchannel flows.

To account for the effects of the rectangular geometry, three-sided wall heating, and multichannel interactions in a heat sink, Lee and Mudawar [68] modified the Hall and Mudawar ultra-high CHF formulation for small tubes [29], recommending the following correlation:

$$q''_{p,m} = 0.0332\, Gh_{fg}\mathrm{We}_{D_{eq}}^{-0.114}\left(\frac{\upsilon_g}{\upsilon_f}\right)^{-0.681}\left[1 + 0.684\left(\frac{\upsilon_g}{\upsilon_f}\right)^{0.832}\frac{\Delta h_{\mathrm{sub},in}}{h_{fg}}\right]\left[1 + 0.0908\ \mathrm{We}_{D_{eq}}^{-0.235}\left(\frac{\upsilon_g}{\upsilon_f}\right)^{0.151}\frac{L}{D_{eq}}\right]^{-1} \tag{31}$$

where

$$D_{eq} = \frac{D_h}{\mathrm{Nu}_3/4.364}, \mathrm{We}_{D_{eq}} = \frac{G^2 D_{eq}}{\sigma\rho_f} \tag{32}$$

and q''_{pm} is the average CHF along the heated walls of the microchannel.

3.10 Premature Critical Heat Flux. Premature CHF is a serious limit to the cooling performance of a two-phase microchannel heat sink. It is closely associated with the two-phase flow instabilities discussed in Sec. 3.6. This phenomenon is encountered mostly at low mass velocities, where a larger volume of vapor is produced inside the microchannels for a given inlet temperature and heat flux [67,120]. Figure 23 shows sequential images of vapor behavior in the upstream portion of a heat sink containing 11 of 259.9 μm $\times$ 1041.3 μm channels equally distributed along a 0.50 cm wide by 1.0 cm long heated surface and using HFE 7100 as working fluid [67]. These images were obtained at a relatively low mass velocity of $G = 670$ kg/m^{2}s, an inlet temperature of 0 °C (subcooled flow), and a base heat flux just exceeding 250 W/cm^2. Low mass velocity results in slug and even annular flow as far upstream as the inlet. At this low mass velocity, the momentum of incoming liquid from the upstream plenum is momentarily too weak to overcome the relatively high pressure drop across the channel resulting from the high vapor production. This causes vapor from the microchannels to flow backward toward the inlet plenum. Vapor from adjacent microchannels begins to coalesce into one large vapor volume inside the inlet plenum, momentarily blocking any liquid flow into the microchannels, and causing temporary dryout and temperature rise in the microchannels. This causes the upstream plenum pressure to rise gradually until it is able to push all the coalescent vapor volume downstream through the microchannels, providing partial wetting of the microchannel walls and reducing the wall temperature. With liquid now flowing through the microchannels, vapor can be generated in the microchannels once more, initiating a new build-up/purge cycle. This cycle occurs with high frequency and is associated with large fluctuations in both pressure and temperature, but the mean temperature increases with each new cycle.

There are two effective means to overcoming premature CHF [67]. The first is to increase mass velocity to prevent vapor backflow in the first place. The second is to supply the coolant more subcooled to capitalize on condensation effects and to reduce bubble growth and coalescence.

4 Assessment of Heat Transfer Enhancement Schemes

4.1 Optimization of Microchannel Geometry. A designer of a two-phase microchannel heat sink is often faced with the task of choosing a microchannel geometry and assign operating conditions that yield the highest possible two-phase heat transfer coefficient and CHF and lowest pressure drop corresponding to a given heat flux and coolant flow rate. In arriving at an optimal design, one has to examine three types of parameters: geometrical parameters, operating parameters, and thermal/fluid parameters. Geometrical parameters consist of the heat sink and microchannel dimensions. Operating parameters include coolant, inlet temperature and pressure, and flow rate. Thermal/fluid parameters are

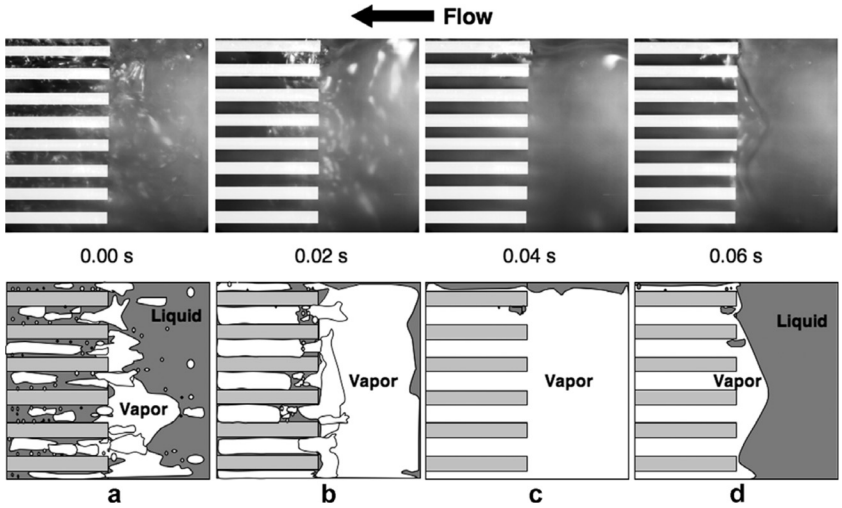

Fig. 23 Premature CHF and flow oscillations in heat sink with $D_h = 415.9\,\mu m$ for $T_{in} = 0^\circ C$, $G = 670\,kg/m^2\,s$, and $q''_{base} > 250.0\,W/cm^2$: (*a*) initial vapor pocket buildup in upstream plenum, (*b*) growth of vapor mass, (*c*) complete blockage of inlet plenum by vapor mass, and (*d*) purging of vapor mass along microchannels. (Adapted from Lee and Mudawar [67])

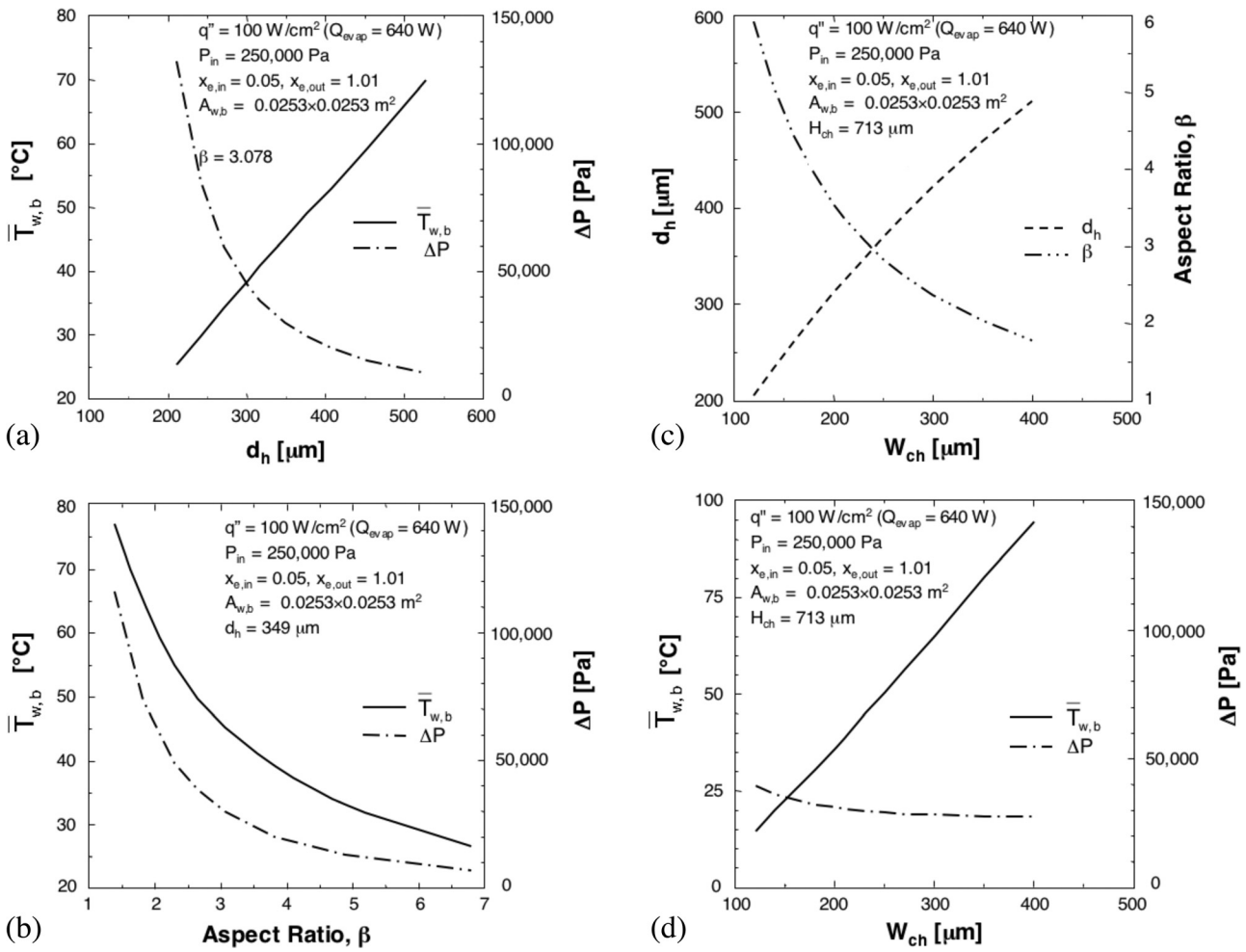

Fig. 24 (*a*) Variations of mean microchannel base temperature and pressure drop with hydraulic diameter. (*b*) Variations of mean microchannel base temperature and pressure drop with channel aspect ratio. (*c*) Variations of hydraulic diameter and aspect ratio with channel width for constant channel height. (*b*) Variations of mean channel base temperature and pressure drop with channel width for constant channel height. All results are based on channel wall thickness equal to channel width. (Adapted from Lee and Mudawar [150]).

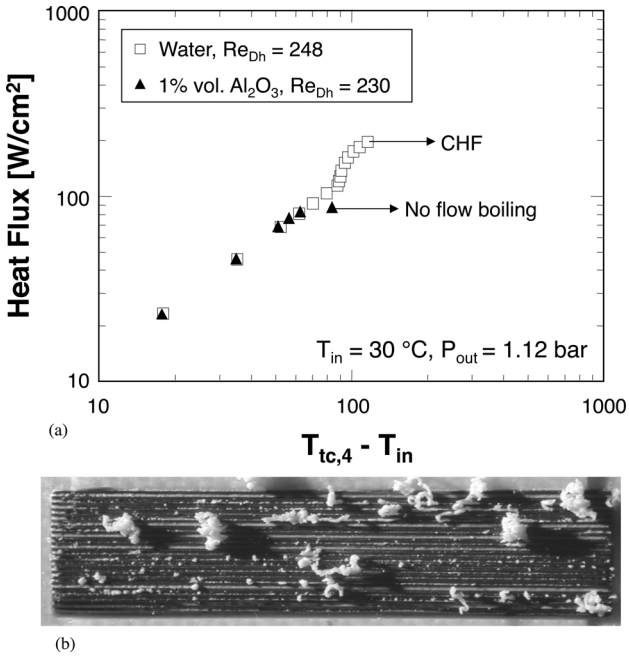

Fig. 25 (*a*) Flow boiling curve at measurement downstream location tc4 for pure water and 1% Al_2O_3. (*b*) Photograph of particles after being removed from microchannels. (Adapted from Lee and Mudawar [154])

output parameters that describe the transport behavior of the heat sink and, whose magnitude is used to guide the designer in selecting optimum microchannel dimensions.

Qu and Mudawar [149] explored two separate methods to optimizing heat sink geometry. The first corresponds to fixed values of heat flux and coolant flow rate and yields operating conditions that provide acceptable combinations of pressure drop and heat sink base temperature. The second is based on a fixed heat flux and pressure drop and is used to determine acceptable combinations of coolant flow rate and heat sink base temperature.

Lee and Mudawar [150] provided a comprehensive methodology to optimizing cooling performance relative to the heat sink's geometrical parameters using two-phase pressure drop and heat transfer correlations they developed in a prior study [64,65]. A heat sink containing rectangular microchannels with height H_{ch} and width W_{ch} was configured to cool the surface of a 2.53×2.53 cm^2 device dissipating $100\,W/cm^2$ using R134a. The heat sink was used as an evaporator in a vapor compression cycle. The refrigerant was assumed to enter the heat sink at $P_{in} = 2.5 \times 10^5$ Pa as a two-phase mixture with a quality of $x_{e,in} = 0.05$. To ensure acceptable compressor operation and a good coefficient of performance while avoiding appreciable outlet wall temperature rise, the outlet quality was set at $x_{e,out} = 1.01$. They also assumed a channel wall thickness equal to the channel width, W_{ch}. Figure 24(*a*) shows that decreasing hydraulic diameter, d_h, for a fixed channel aspect ratio β ($= H_{ch}/W_{ch}$) reduces the wall temperature. However, a smaller diameter can increase pressure drop appreciably. Figure 24(*b*) shows that increasing the channel's aspect ratio for a constant hydraulic diameter reduces wall temperature and pressure drop concurrently. Figure 24(*c*) shows how the aspect

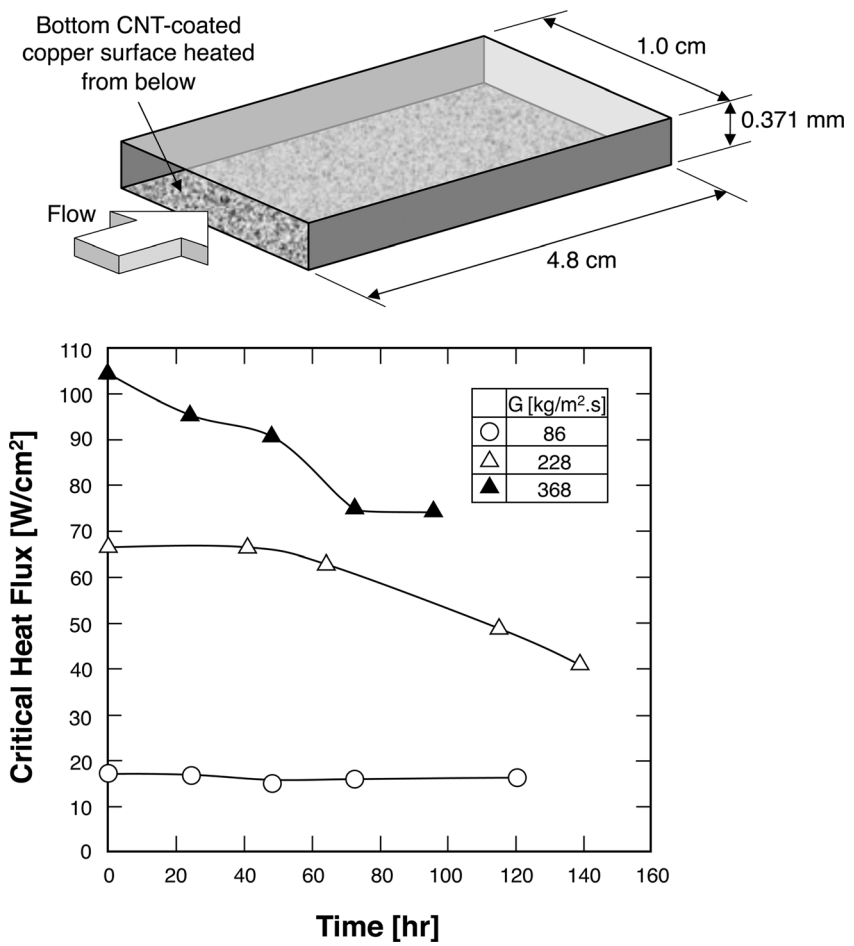

Fig. 26 Variation of CHF with time for CNT-coated surfaces for three mass velocities and $T_{in} = 30^\circ C$. (Adapted from Khanikar et al. [158])

ratio can be increased and hydraulic diameter decreased for a fixed channel height, H_{ch}, by reducing the channel width. Finally, Fig. 24(*d*) shows that by decreasing the channel width, the wall temperature can be decreased, mostly because of a smaller hydraulic diameter. By maintaining a high aspect ratio, the same decrease in channel width yields only a modest increase in pressure drop. These trends highlight a very important strategy in designing two-phase microchannel heat sinks: using narrow microchannels with high aspect ratio.

4.2 Assessment of Merits of Nanoparticles. Because of the superior conductivity of solid particles compared to common heat transfer liquids, mixing solid particles in the liquid has been recommended as a means to enhancing the cooling potential of the liquid. This became more feasible following recent developments in nanotechnology and related manufacturing techniques, which made possible the production of nanosized particles. The term "nanofluids," which refers to a fluid-nanoparticles mixture, was coined by Choi and co-workers at Argonne National Laboratory who proposed the use of nanoparticles to enhance the thermal conductivity of liquids [151]. Lee et al. [152] demonstrated this thermal conductivity enhancement using 50 nm or smaller Al_2O_3 and CuO particles. They showed that the enhancement was not only a function of particle conductivity and concentration but also particle size and shape. Xue [153] showed analytically that carbon nanotubes produce the highest conductivity enhancement of all nanofluids.

Lee and Mudawar [154] investigated the effectiveness of 1% and 2% Al_2O_3 nanoparticle volumetric concentrations at enhancing single-phase and two-phase heat transfer of water through a heat sink containing 21 of 215 μm wide by 821 μm deep rectangular microchannels. While the high thermal conductivity of nanoparticles did enhance the single-phase heat transfer coefficient for fully developed laminar flow, the enhancement was much weaker for turbulent flow because of the weaker dependence of the heat transfer coefficient on thermal conductivity as well as decreased specific heat and increased viscosity with increased nanoparticle concentration. Increasing the Al_2O_3 concentration also increased the single-phase pressure drop compared to pure water at the same Reynolds number. Practical long-term concerns were raised concerning the use of nanoparticles, including particle settling (which can yield undesirable concentration gradients), abrasion to the surfaces of flow loop components, and more importantly, potential clogging of microchannels, valves, and pump passages.

Nanoparticles had a very detrimental effect during flow boiling. Shortly after boiling commenced inside the microchannels, localized evaporation caused particles to deposit into relatively large clusters near the channel exit. This clustering phenomenon quickly propagated upstream, filling the entire channel and preventing coolant from entering the heat sink. This resulted in catastrophic failure of the heat sink in the form of a very premature CHF as shown in Fig. 25(*a*). Figure 25(*b*) shows photographs of the particle clusters after they were removed from the microchannels with the aid of a fine needle. These findings prove that nanofluids should be avoided in two-phase microchannel applications.

4.3 Assessment of Merits of Carbon Nanotubes. Carbon nanotubes (CNTs) take the shape of extremely thin tubes of graphitic carbon with typical outer diameters ranging from 1 to 100 nm and lengths from 1 to 50 μm. They exist in single-walled (SWCNT) or multiwalled (MWCNT) forms. SWCNTs are made from a single graphene sheet with hexagonally arranged groups of carbon atoms, whereas MWCNTs have multiple co-axial graphene sheets. Kim et al. [155] showed that MWCNTs possess thermal conductivities in excess of 3000 W/m K at room temperature, which explains the recent strong interest in implementing CNTs in cooling applications.

Ujereh et al. [156] explored the enhancement benefits of CNTs in pool boiling of FC-72 on silicon and copper surfaces. Compared to bare substrates, CNT-coated surfaces reduced the incipient boiling superheat and enhanced the nucleate boiling heat transfer coefficient. These advantages were explained by the effectiveness of CNTs at both initiating and sustaining the nucleation process, in addition to the increased surface area. With CNTs, vapor entrapment was improved with the creation of near zero angle cavities between parallel vertical CNTs and CNT mesh formations. CHF was also increased with CNT coatings for both silicon and copper substrates because of the increased surface area. Launay et al. [157] also achieved pool boiling heat transfer enhancement with PF-5060 on CNT coating when compared with bare silicon. However, CNTs degraded performance close to CHF. Performance differences between the studies of Ujereh et al. and Launay et al. can be attributed to differences in the CNT growth process and anchoring to the surface, which have a strong bearing on contact resistance.

Recently, Khanikar et al. [158] performed experiments to assess the heat transfer enhancement benefits of coating the bottom wall of a rectangular 10.0-mm wide by 0.371-mm high microchannel with carbon nanotubes (CNTs). The tests were performed with water on a bare copper surface and three separate yet identical CNT-coated surfaces. Each of the CNT-coated surfaces was subjected to repeated boiling tests at the same mass velocity to explore any time dependence of heat transfer performance parameters. The influence of CNT coating was markedly different at high mass velocities as compared to low. As shown in Fig. 26, CHF was fairly constant at low mass velocities but degraded following repeated tests at high mass velocities, proving high flow velocities cause appreciable changes to the morphology of the CNT-coated surface. The SEM images in Fig. 27 show the initially near-vertical, CNTs were bent upon the heated surface at high mass velocities to form a dominant "fish-scale" pattern. Voids between the fish scales provided near-zero-angle cavities that enhanced heat transfer in the nucleate boiling region compared to the bare copper surface. While CHF did increase because of the increased heat transfer area associated with the CNT coating, the increase was compromised following repeated tests, as the CNT fin effect was lost due to the bending.

These findings bring into question the overall effectiveness of using CNTs to enhance flow boiling in microchannels, especially that they are most problematic at high mass velocities that are generally sought to achieve superior flow boiling performance in microchannels.

4.4 Parallel-Channel Enhancement: Smart Pumpless Loops. Reliability concerns drive many electronics cooling systems away from the use of mechanical pumps to circulate liquid coolant. This is a key reason behind the reliance on "passive cooling" devices such as heat pipes in many electronics applications. But, while heat pipes do offer many advantages, such as compactness, low cost, and reliability, which are important to many applications, such as notebook computers, they are no longer able to handle anticipated heat dissipation requirements of advanced processors. This limitation is caused by the miniscule liquid flow rates a heat pipe's wick can deliver by capillary forces. This limitation is eliminated with the use of another passive cooling system, the thermosyphon. Here, fluid motion is achieved by buoyancy. The heat-dissipating device is fully submerged in a pool of liquid coolant and vapor released by nucleate boiling rises by buoyancy to the upper region of the thermosyphon. The vapor is returned to liquid state by condensation on the surfaces of an air-cooled condenser and drips back to the liquid pool below. But, while thermosyphons provide better cooling performance than heat pipes, they suffer from relatively a low CHF [159]. For example, CHF for saturated boiling, according to the Zuber et al. [35] model, is 15.24 W/cm^2 for FC-72 and 110.4 W/cm^2 for water.

Mukherjee and Mudawar [160,161] developed a new passive cooling technique that can yield far better cooling rates than thermosyphons. The system they developed utilizes fluid density

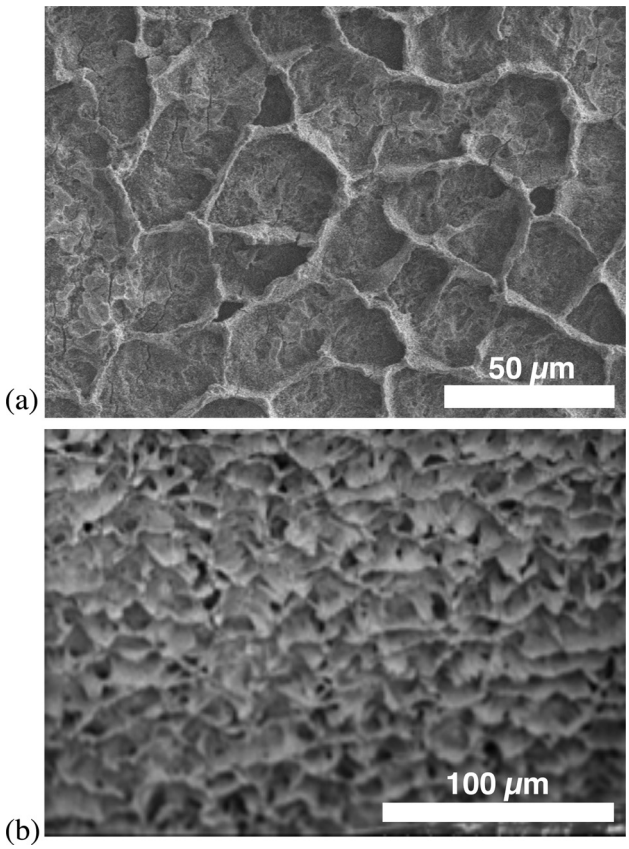

Fig. 27 SEM images of CNT-coated surface after five boiling tests at $G = 368\,kg/m^2$ s and $T_{in} = 30°C$. (*a*) CNT cellular formations observed over isolated regions of the surface. (*b*) Dominant fish-scale pattern observed over most of the surface. (Adapted from Khanikar et al. [158])

differences between two vertical, parallel tubes to achieve coolant flow. Depicted in Fig. 28, the two tubes are connected at the top to a free-surface reservoir, which is fitted with an air-cooled condenser above, and the heat-dissipating device is incorporated into a boiler at the bottom of the "hot tube." Motion is induced in the system when nucleate boiling occurs in the hot tube and bubbles are driven upward by buoyancy. High void fraction decreases the mixture density in the hot tube, while the other "cold tube" maintains a fairly constant liquid density. A substantial nonequilibrium in hydrostatic pressure is induced which, in the presence of a free interface in the reservoir, produces higher pressure at the bottom of the cold tube compared to the hot tube. This pressure difference sets up a clockwise fluid motion, where liquid is drawn downward from the reservoir through the cold tube as a two-phase mixture travels upward in the hot tube. A key advantage of this system compared to the thermosyphon is that it separates the path of the replenishment liquid from that of the released vapor, enabling it to achieve higher CHF values.

Aside from being passive (i.e., does not require a mechanical pump to achieve coolant motion), this system is "smart," in the sense that it improves its own performance without external control input in response to an increasing heat load. This behavior can be explained as follows. As the heat input increases in the boiler, increased vapor production in the hot tube increases the density difference between the two tubes, thereby accelerating coolant circulation and increasing the system's cooling capacity. Interestingly, the density differences between the two tubes can be greatly increased by reducing both flow passage area in the boiler (i.e., using microchannel flow) and the diameters of the two tubes; both of which lead to a more compact cooling system design. However, for the coolant acceleration to be achieved, the induced nonequilibrium in static pressure must be able to overcome the increased frictional pressure gradients in the two tubes as well as the accelerational pressure gradient in the hot tube.

To assess the effectiveness of a microchannel boiler at both overcoming these pressure gradients and achieving superior cooling performance compared to thermosyphons, Mukherjee and Mudawar [160,161] tested this concept with both FC-72 and water

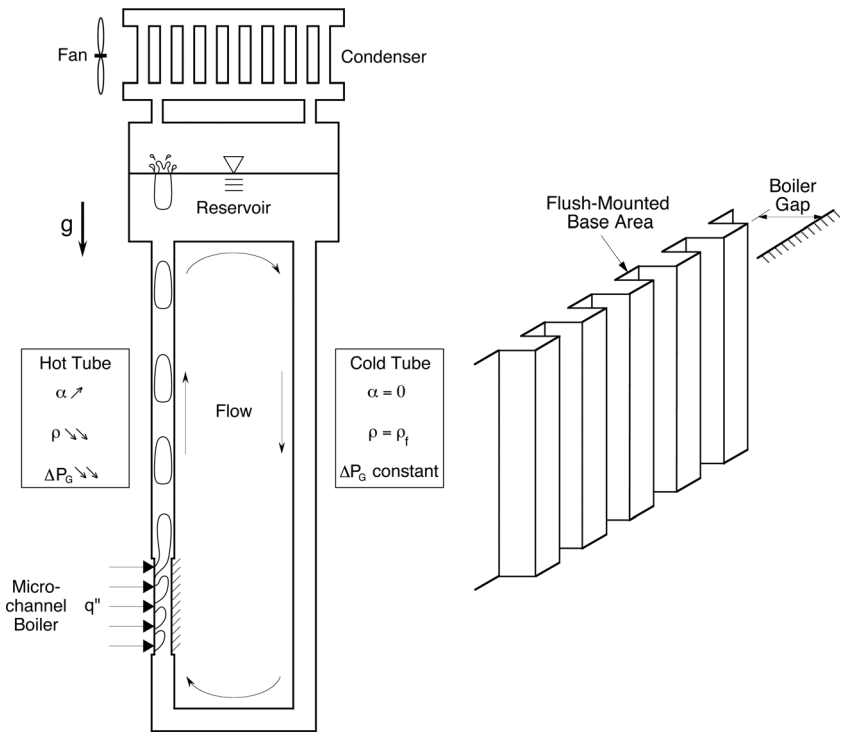

Fig. 28 Smart, passive (pump-free) cooling concept and boiler microchannel enhancement features. (Adapted from Mukherjee and Mudawar [160,161]).

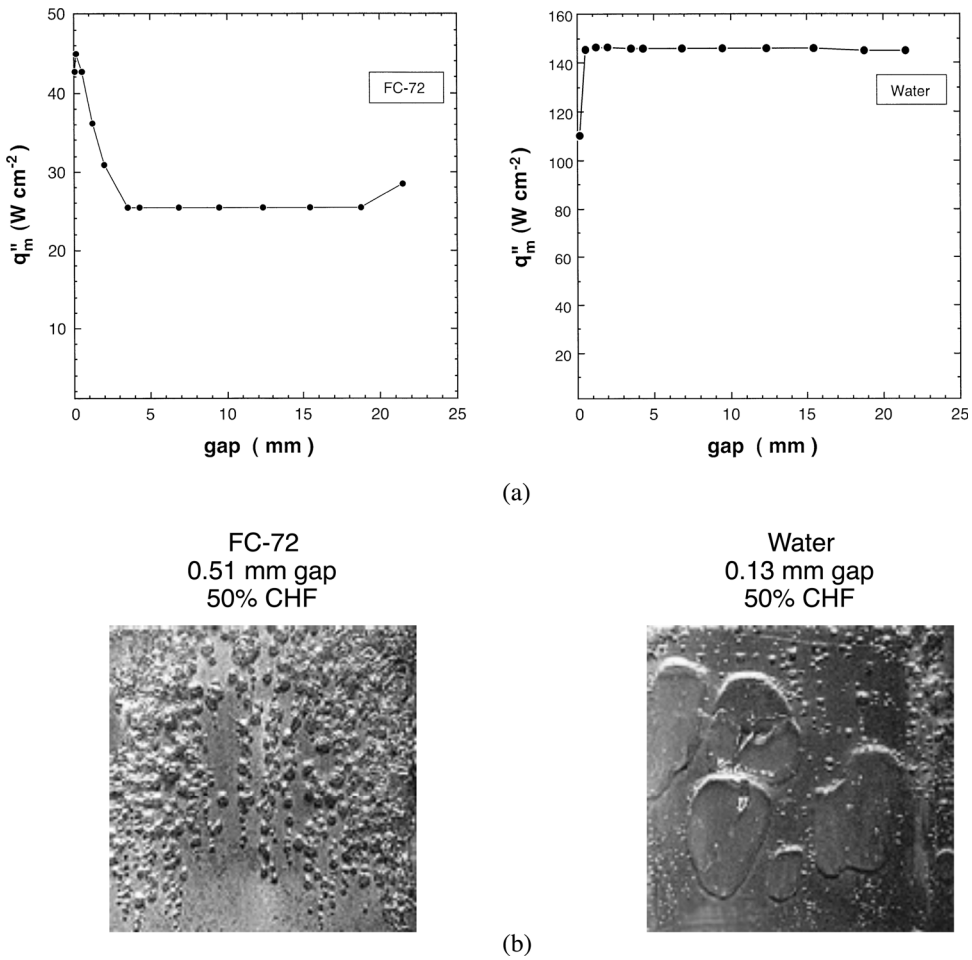

Fig. 29 (*a*) Comparison of pumpless loop CHF variation with gap width for FC-72 and water. (*b*) Photographs of nucleate boiling in FC-72 and in water. (Adapted from Mukherjee and Mudawar [160,161])

by varying the "boiler gap" from 0.051 to 21.46 mm as well as using boiler surfaces with vertical microchannels. For large gaps, CHF was fairly insensitive to gap width for both fluids. However, small gaps produced opposite trends for the two fluids. As shown in Fig. 29(*a*), decreasing the gap below 3.56 mm produced a substantial rise in CHF for FC-72, reaching a maximum for a 0.13 mm gap. For water, Fig. 29(*a*), CHF was fairly insensitive down to 0.51 mm, below which it began to decrease sharply. These trends were proven to be closely related to the small surface tension and contact angle of FC-72 producing very small bubbles that could easily pass through narrow gaps, whereas much larger bubbles in water obstruct liquid replenishment in narrow gaps as illustrated in Fig. 29(*b*). To contrast the system's performance with those of compact thermosyphons, CHF was also measured in pool boiling for both fluids corresponding to the same boiler gaps. These tests yielded greatly reduced pool boiling CHF values with small gaps compared to an infinite liquid pool. In fact, CHF multiples as high as 4.5 and 4.2 were realized with the pumpless loop

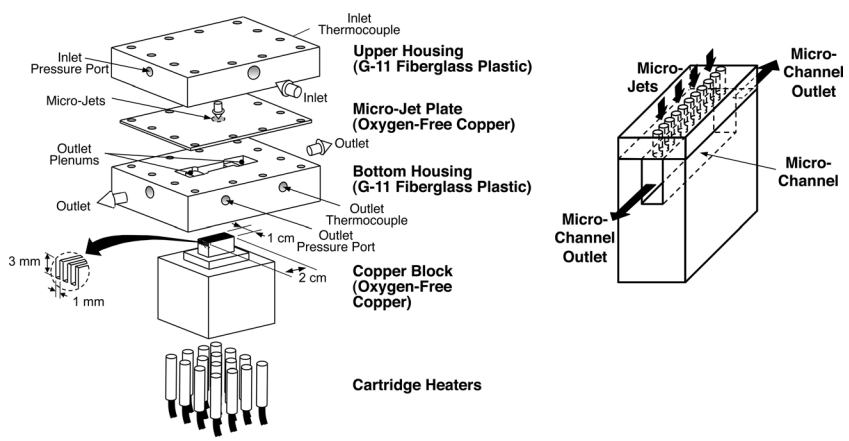

Fig. 30 Construction of hybrid microchannel/jet-impingement cooling module [164,165]

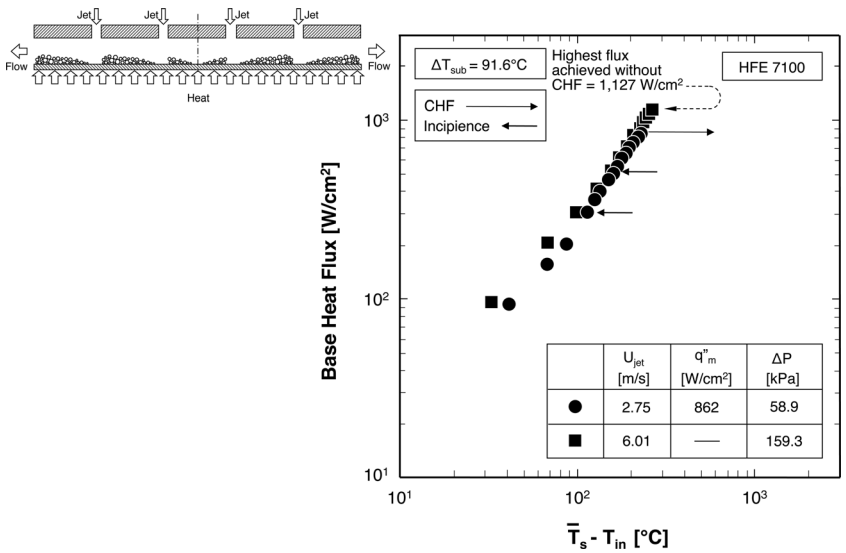

Fig. 31 Schematic representation of vapor growth along microchannel in hybrid microchannel/jet-impingement cooling module, and boiling curves corresponding to two jet velocities. (Adapted from Sung and Mudawar [167])

technique compared to pool boiling with identical gaps for FC-72 and water, respectively. A numerical model was constructed to determine how the gap influences the various components of pressure drop, velocities, coolant flow rate, and hence system response to heat input.

4.5 Performance Enhancement Using Hybrid Cooling Schemes. Hybrid cooling is a concept that was developed in response to the need to tackle high heat fluxes from advanced defense devices found in radars and directed-energy laser and microwave weapon systems, which are projected to exceed 1000 W/cm^2 [1]. Such heat dissipation exceeds the capabilities of today's two most advanced dielectric liquid cooling schemes, microchannel and jet impingement. While two-phase microchannel heat sinks offer many desirable features, such as small size and weight, minimal coolant inventory, and high convective heat transfer coefficients, they can produce high pressure drop and appreciable temperature gradients along the direction of coolant flow when dissipating very high heat fluxes. Jet impingement is known to produce high heat transfer coefficients in the impingement zone and require smaller pressure drop than microchannels, but they also produce large surface temperature gradients away from the impingement zone. Use of multiple impinging jets can diffuse temperature gradients over large surface areas, but this both greatly increases coolant flow rate and complicates the routing of spent coolant between impingement zones.

Loosely based on a concept originally proposed by Mudawar and Wadsworth [162,163], Sung and Mudawar [64,65] proposed combining the cooling benefits of microchannels and jet-impingement in a "hybrid" cooling module. As shown in Fig. 30, the coolant is introduced gradually into each microchannel in the form of small circular (or slot) jets, capitalizing upon the high-heat-flux removal capabilities of both jet impingement and microchannel flow, while decreasing both the temperature gradients along the microchannel and pressure drop. The hybrid module is also very effective at controlling the flow of spent fluid downstream of the impingement zones of the jets. They tested a hybrid module that featured five 1-mm wide and 3-mm deep microchannels that spanned a $1.0 \times 2.0\,\text{cm}^2$ heated surface using HFE 7100 as working fluid. Different jet configurations were tested and compared to a configuration consisting of five parallel arrays of 14 0.39-mm diameter circular holes. For all configurations, increasing the coolant's flow rate delayed the onset of boiling and increased CHF. Increasing the subcooling increased CHF considerably by enabling the liquid to absorb an appreciable fraction of the supplied heat in the form of sensible energy prior to evaporation [166].

Figure 31 illustrates one of the key heat transfer merits of the hybrid module. Unlike conventional microchannel heat sinks, where void fraction increases monotonically along the flow direction, producing undesirable increases in both pressure and temperature gradients, the hybrid module produces a repeated pattern of bubble growth and collapse between jets that nets only a mild overall increase in vapor void fraction. This also facilitates better utilization of the coolant's subcooling everywhere along the microchannel. This is evidenced by the module's ability to achieve an unprecedented heat flux of 1127 W/cm^2 as shown in Fig. 31. This particular test was actually terminated at this heat flux without incurring CHF. These findings demonstrate the enormous cooling potential of hybrid two-phase cooling schemes.

A recent study by Ndao et al. [168] provides a useful background on different phase change electronic cooling techniques, which may provide some guidance in combining the merits of different techniques in pursuit of superior cooling performance.

5 Closing Remarks

This paper addressed the broad range of applications of two-phase microchannel heat sinks, the current understanding of their transport behavior, and effective means to enhance their performance. While most researchers associate these heat sinks exclusively with computer cooling, this study highlights the versatility of these devices at tackling cooling needs in numerous other applications.

Despite the large number of published articles on two-phase microchannel heat sinks, there is a shortage of reliable predictive tools for certain performance parameters. This shortage stems from a lack of reliable databases that are essential to the development of models and correlations. Such databases must encompass broad ranges of operating and geometrical parameters as well as fluids with drastically different thermophysical properties. Additionally, they must relate individual data to clearly define two-phase flow regimes and distinguish between subcooled and saturated operating conditions. There is also a need for careful assessment of heat loss in databases. One noteworthy weakness in much of the literature is the quest for correlations that are not based on physical dimensionless groups that capture microchannel flow boiling behavior.

This study also showed that cutting-edge heat transfer enhancement techniques with proven merits to macro systems may not

offer similar advantages to microchannel heat sinks. Rather, careful optimization of the heat sink's geometrical parameters may yield better performance enhancement. New innovative enhancement methods, especially those that combine the benefits of microchannel flow with those of jet impingement—hybrid cooling schemes—may alleviate some of the disadvantages of boiling in small passages and yield unprecedented cooling performances.

Following are specific recommendations to maximize the utilization of both prior and future studies.

(1) The heat transfer community must pursue efforts to systematically consolidate published databases for pressure drop, heat transfer coefficient, and CHF for flow boiling in microchannels.
(2) Consolidated databases will be highly instrumental in identifying major "gaps" in experimental data relative to coolant type and thermophysical properties, pressure, mass velocity, quality, microchannel size and shape, and length-to-hydraulic diameter ratio. This would help steer experimental studies in a direction that maximizes the usefulness and overall impact and reduces unnecessary investment in future experimental work.
(3) Consolidated databases will also serve to identify any potential errors in published databases due to such factors as absence of heat loss analysis. By filtering out erroneous data or entire databases, it may be possible to achieve a more accurate and useful set of consolidated databases.
(4) Consolidated databases with broad coverage of coolant thermophysical properties, pressure, mass velocity, quality, quality, microchannel size and shape, and length-to-hydraulic diameter ratio will serve as a powerful foundation for developing both universal correlations and physics-based models.
(5) Efforts should also be made to review and consolidate published models for pressure drop, heat transfer coefficient, and CHF for flow boiling in both microchannel and macrochannel flows, including studies beyond those intended solely for electronic cooling. While studies have shown that macrochannel predictive tools may not be applicable to microchannels, our present understanding of two-phase flow and heat transfer is derived mostly from macrochannel literature. Clearly, macrochannel models must be carefully ascertained, recognizing the limitations of these models relative to small channel size.
(6) The benefits of microchannel flow boiling should be extended to new applications in the biomedical, pharmaceutical, renewable energy, transportation, aerospace, and defense industries.
(7) Efforts should begin to focus more on hybrid cooling schemes that combine the merits of microchannel flow boiling with those of other powerful cooling schemes, especially jet impingement.

Acknowledgment

The author is grateful for the support of the Office of Naval Research (ONR) for this study.

Nomenclature

A = flow area of microchannel
A_p = projected area of bubble
C = empirical constant
C_D = drag coefficient
C_s = empirical coefficient in Eq. (7)
Ca = Capillary number
Co = Confinement number
D = diameter
D_b = bubble diameter
D_F = friction diameter
D_h = hydraulic diameter
D_{tran} = diameter corresponding to transition from macrobehavior to microbehavior
F_D = drag force on a bubble
f_{fo} = liquid-only friction factor
F_s = surface tension force
f_{tp} = two-phase friction factor
Fr = Froude number
g = body force per unit mass
G = mass velocity (kg/s m^2)
g_e = Earth gravity
h = heat transfer coefficient; enthalpy
H_{ch} = height of microchannel
h_{fg} = latent heat of vaporization
h_{sat} = heat transfer coefficient for saturated boiling
h_{sc} = heat transfer coefficient for subcooled boiling
h_{sp} = heat transfer coefficient for single-phase liquid cooling
Δh_{sub} = enthalpy of subcooling
j_f = superficial liquid velocity
j_g = superficial vapor (or gas) velocity
k_w = thermal conductivity of wall between microchannels
L = length of microchannel; length of microchannel segment
M = two-phase Mach number
n = empirical constant
Nu = Nusselt number
P = pressure
P_c = length of bubble contact line
P_F = friction perimeter of channel
P_H = heated perimeter of channel
Pr = Prandtl number
q_{base} = heat flux based on base area of microchannel heat sink
q_{eff} = heat flux along heated perimeter of microchannel
q_i = incipient boiling heat flux
r_b = radius of departing bubble
Re = Reynolds number
Re_b = bubble Reynolds number; $\rho_f u_e (2r_b)/\mu_f$
Re_{in} = inlet Reynolds number of liquid
Re_{tran} = Reynolds number corresponding to transition from macrobehavior to microbehavior; $(GD_{\text{tran}})/\mu_f$
S = slip ratio
t = time
T = temperature
T_{in} = mean liquid inlet temperature
$\bar{T}_{w,b}$ = mean microchannel base temperature
ΔT_{sub} = subcooling
u = two-phase mixture velocity in HEM model
U = mean liquid velocity
u_e = liquid velocity at point e halfway to bubble tip
u_{in} = mean liquid inlet velocity
v = specific volume
v_{fg} = specific volume difference between vapor and liquid
W_{ch} = width of microchannel
W_w = thickness of wall between microchannels
We = =Weber number
We_{tran} = Weber number corresponding transition from macrobehavior to microbehavior; $(G^2 D_{\text{tran}})/\rho_f \sigma$
x = quality; axial coordinate
X = Lockhart–Martinelli parameter
x_e = thermodynamic equilibrium quality
z = axial coordinate

Greek Symbols

α = void fraction
β = channel aspect ratio
ε = fin effectiveness
θ_0 = equilibrium contact angle
θ_a = advancing contact angle
θ_r = receding contact angle
μ = dynamic viscosity
$\bar{\mu}$ = two-phase mixture viscosity

ρ = density
$\bar{\rho}$ = two-phase mixture density
σ = surface tension
τ_F = frictional shear stress

Subscripts

3 = three-sided heating
4 = four-sided heating
A = accelerational
b = bubble
c = channel centerline
ch = microchannel
cor = correlation
eq = equivalent
f = liquid; saturated liquid
F = frictional
fo = liquid only
g = saturated vapor
G = gravitational
H = heated
i = inlet
in = channel inlet
jet = jet
m = maximum, CHF
out = channel outlet
sat = saturated
sp = single-phase
sub = subcooled
tp = two phase
tran = transitional
w = wall between microchannels

References

[1] Mudawar, I., 2001, "Assessment of High-Heat-Flux Thermal Management Schemes," IEEE Trans. Compon. Packag. Manuf. Technol., **24**, pp. 122–141.
[2] Tuckerman, D. B., and Pease, R. F. W., 1981, "High-Performance Heat Sinking for VLSI," IEEE Electronic Devices Lett., **2**, pp. 126–129.
[3] Kishimito, T., and Ohsaki, T., 1986, "VLSI Packaging Technique Using Liquid-Cooled Channels," IEEE Trans. Compon., Hybrids, Manuf. Technol., **9**, pp. 328–335.
[4] Phillips, R. J., 1990, "Micro-Channel Heat Sinks," *Advances in Thermal Modeling of Electronic Components*, A. Bar-Cohen and A. D. Kraus, eds., ASME, New York, NY., Vol. 2, pp. 109–184.
[5] Copeland, D., Takahira, H., Nakayama, W., and Pak, B. C., 1995, "Manifold Microchannel Heat Sinks: Theory and Experiment," *Advances in Electronic Packaging, EEP-Vol. 10*, ASME, pp. 829–835.
[6] Choquette, S. F., Faghri, M., Charmchi, M., and Asako, Y., 1996, "Optimum Design of Microchannel Heat Sinks," *Micro-Electro-Mechanical Syst.ems (MEMS)*, DSC-Vol. 59, ASME, pp. 115–126.
[7] Yin, X., and Bau, H. H., 1997, "Uniform Channel Micro Heat Exchangers," ASME J. Electron. Packag., **119**, pp. 89–93.
[8] Kawano, K., Minakami, K., Iwasaki, H., and Ishizuka, M., 1998, "Micro Channel Heat Exchanger for Cooling Electrical Equipment," *Application of Heat Transfer in Equipment, Systems and Education, HTD-Vol. 361-3/PID-Vol. 3*, ASME, pp. 173–180.
[9] Lee, D. Y., and Vafai, K., 1999, "Comparative Analysis of Jet Impingement and Microchannel Cooling for High Heat Flux Applications," Int. J. Heat Mass Transfer, **42**, pp. 1555–1568.
[10] Fedorov, A. G., and Viskanta, R., 2000, "Three-Dimensional Conjugate Heat Transfer in the Microchannel Heat Sink for Electronic Packaging," Int. J. Heat Mass Transfer, **43**, pp. 399–415.
[11] Qu, W., and Mudawar, I., 2000, "Experimental and Numerical Study of Pressure Drop and Heat Transfer in a Single-Phase Micro-Channel Heat Sink," Int. J. Heat Mass Transfer, **45**, pp. 2549–2565.
[12] Qu, W., and Mudawar, I., 2002, "Analysis of Three-Dimensional Heat Transfer in Micro-Channel Heat Sinks," Int. J. Heat Mass Transfer, **45**, pp. 3973–3985.
[13] Bowers, M. B., and Mudawar, I., 1994, "High Flux Boiling in Low Flow Rate, Low Pressure Drop Mini-Channel and Micro-Channel Heat Sinks," Int. J. Heat Mass Transfer, **37**, pp. 321–332.
[14] Bowers, M. B., and Mudawar, I., 1994, "Two-Phase Electronic Cooling Using Mini-Channel and Micro-Channel Heat Sinks—Part 1. Design Criteria and Heat Diffusion Constraints," ASME J. Electron. Packag., **116**, pp. 290–297.
[15] Bowers, M. B., and Mudawar, I., 1994, "Two-Phase Electronic Cooling Using Mini-Channel and Micro-Channel Heat Sinks—Part 2. Flow Rate and Pressure Drop Constraints," ASME J. Electron. Packag., **116**, pp. 298–305.
[16] Qu, W., and Mudawar, I., 2004, "Transport Phenomena in Two-Phase Micro-Channel Heat Sinks," ASME J. Electron. Packag., **126**, pp. 213–224.
[17] Wallis, G. B., 1969, *One Dimensional Two-Phase Flow*, 2nd ed., McGraw-Hill, New York, NY.
[18] Koskie, J. E., Mudawar, I., and Tiederman, W. G., 1989, "Parallel-Wire Probes for Measurement of Thick Liquid Films," Int. J. Multiphase Flow, pp. 521–530.
[19] El-Masri, M. A., and Louis, J. F., 1978, "On the Design of High-Temperature Gas Turbine Blade Water Cooling Channels," ASME J. Eng. Power, **100**, pp. 586–591.
[20] Kydd, P. H., and Day, W. H., 1975, "An Ultra High Temperature Turbine for Maximum Performance and Fuels Flexibility," ASME Paper No. 75-GT-81.
[21] Caruvana, A., Manning, G. B., Day, W. H., and Sheldon, R. C., 1978, "Evaluation of a Water-Cooled Gas Turbine Combined Cycle Plant," ASME Paper No. 78-GT-77.
[22] Mudawar, I., and El-Masri, M. A., 1984, "Thermal Design Constraints in Open Loop Water-Cooled Turbine Blades," ASME Paper No. 84-WA/HT-68.
[23] Mudawar, I., El-Masri, M. A., Wu, C. S., and Ausman-Mudawar, J. R., 1985, "Boiling Heat Transfer and Critical Heat Flux in High-Speed Rotating Liquid Films," Int. J. Heat Mass Transfer, **28**, pp. 795–806.
[24] Mudawar, I., and El-Masri, M. A., 1988, "Boiling Incipience in Plane Rotating Water Films," ASME J. Heat Transfer, **110**, pp. 532–535.
[25] The European Joint Undertaking for ITER and Development of Fusion Energy, 2008, "Fusion for Energy," Annual Report, Barcelona, Spain.
[26] Boyd, R. D., 1985, "Subcooled Flow Boiling Critical Heat Flux (CHF) and Its Application to Fusion Energy Components—Part I. A Review of Fundamentals of CHF and related Data Base," Fusion Technol., **7**, pp. 7–31.
[27] Mudawar, I., and Bowers, M. B., 1999, "Ultra-High Critical Heat Flux (CHF) for Subcooled Water Flow Boiling—I. CHF Data and Parametric Effects for Small Diameter Tubes," Int. J. Heat Mass Transfer, **42**, pp. 1405–1428.
[28] Ornatskii, A. P., and Vinyarskii, L. S., 1965, "Heat Transfer Crisis in a Forced Flow of Underheated Water in Small-Bore Tubes," Teplofizika Vys. Temp., **3**, pp. 444–451 (Also in High Temperature, **3**, pp. 400–406).
[29] Hall, D. D., and Mudawar, I., 1999, "Ultra-High Critical Heat Flux (CHF) for Subcooled Water Flow Boiling—II. High-CHF Database and Design Parameters," Int. J. Heat Mass Transfer, **42**, pp. 1429–1456.
[30] Wang, Q., Wu, F., Zeng, M., and Luo, L., 2006, "Numerical Simulation and Optimization on Heat Transfer and Fluid Flow of Liquid Rocket Engine Thrust Chamber," Int. J. Comput.-Aided Eng. Softw., **23**, pp. 907–921.
[31] Incropera, F. P., and Dewitt, D. P., 2002, *Fundamentals of Heat and Mass Transfer*, 5th ed., Wiley, New York, NY.
[32] Wadel, M. F., 1998, "Comparison of High Aspect Ratio Cooling Channel Designs for a Rocket Combustion Chamber With Development of an Optimized Design," Cleveland, OH, NASA Technical Report No. TM-1998-206313.
[33] Gambill, W. R., and Green, N. D., 1958, "Boiling Burnout With Water in Vortex Flow," Chem. Eng. Prog., **54**, pp. 68–76.
[34] Gu, C. B., Chow, L. C., and Beam, J. E., 1989, "Flow Boiling in a Curved Channel," *Heat Transfer in High Energy/High Heat Flux Applications*, R. J. Goldstein, L. C. Chow, and E. E. Anderson, eds., ASME, HTD, Vol. 119, pp. 25–32.
[35] Zuber, N., Tribus, M., and Westwater, J. M., 1961, "The Hydrodynamic Crisis in Pool Boiling of Saturated and Subcooled Liquids," *Proceedings of the 1961-62 International Heat Transfer Conference*, Boulder, CO, pp. 230–236.
[36] Sturgis, J. C., and Mudawar, I., 1999, "Critical Heat Flux in a Long, Curved Channel Subjected to Concave Heating," Int. J. Heat Mass Transfer, **42**, pp. 3831–3848.
[37] Sturgis, J. C., and Mudawar, I., 1999, "Assessment of CHF Enhancement Mechanisms in a Curved, Rectangular Channel Subjected to Concave Heating," ASME J. Heat Transfer, **121**, pp. 394–404.
[38] Mudawar, I., Howard, A. H., and Gersey, C. O., 1997, "An Analytical Model for Near-Saturated Pool Boiling CHF on Vertical Surfaces," Int. J. Heat Mass Transfer, **40**, pp. 2327–2339.
[39] Howard, A. H., and Mudawar, I., 1999, "Orientation Effects on Pool Boiling CHF and Modeling of CHF for Near-Vertical Surfaces," Int. J. Heat Mass Transfer, **42**, pp. 1665–1688.
[40] Galloway, J. E., and Mudawar, I., 1993, "CHF Mechanism in Flow Boiling From a Short Heated Wall-Part 1. Examination of Near-Wall Conditions With the Aid of Photomicrography and High-Speed Video Imaging," Int. J. Heat Mass Transfer, **36**, pp. 2511–2526.
[41] Galloway, J. E., and Mudawar, I., 1993, "CHF Mechanism in Flow Boiling From a Short Heated Wall-Part 2. Theoretical CHF Model," Int. J. Heat Mass Transfer, **36**, pp. 2527–2540.
[42] Sturgis, J. C., and Mudawar, I., 1999, "Critical Heat Flux in a Long, Rectangular Channel Subjected to One-Sided Heating—I. Flow Visualization," Int. J. Heat Mass Transfer, **42**, pp. 1835–1847.
[43] Sturgis, J. C., and Mudawar, I., 1999, "Critical Heat Flux in a Long, Rectangular Channel Subjected to One-Sided Heating—II. Analysis of CHF Data," Int. J. Heat Mass Transfer, **42**, pp. 1849–1862.
[44] Barwick, M., Midkoff, M., and Seals, D., 1991, "Liquid Flow-Through Cooling for Avionics Applications," *Proceedings of the IEEE 1991 National Aerospace and Electronics Conference (NAECON)*, Dayton, OH, Vol. 1, pp. 227–230.
[45] Mudawar, I., Jimenez, P. E., and Morgan, R. E., 1994, "Immersion-Cooled Standard Electronic Clamshell Module: A Building Block for Future High-Flux Avionics Systems," ASME J. Electron. Packag., **116**, pp. 116–125.
[46] Jimenez, P. E., and Mudawar, I., 1994, "A Multi-Kilowatt Immersion-Cooled Standard Electronic Clamshell Module for Future Aircraft Avionics," ASME J. Electron. Packag., **116**, pp. 220–229.

[47] Electrical and Electronics Technical Team, 2006, "Electrical and Electronics Technical Team Roadmap," U.S. Department of Energy, Washington, D.C.
[48] Mudawar, I., Bharathan, D., Kelly, K., and Narumanchi, S., 2009, "Two-Phase Spray Cooling of Hybrid Vehicle Electronics," IEEE Trans. Compon. Packag. Manuf. Technol., **32**, pp. 501–512.
[49] Mori, D., and Hirose, K., 2009, "Recent Challenges of Hydrogen Storage Technologies for Fuel Cell Vehicles," Int. J. Hydrogen Energy, **34**, pp. 4569–4575.
[50] Visaria, M., Mudawar, I., Pourpoint, T., and Kumar, S., 2010, "Study of Heat Transfer and Kinetics Parameters Influencing the Design of Heat Exchangers for Hydrogen Storage in High-Pressure Metal Hydrides," Int. J. Heat Mass Transfer, **53**, pp. 2229–2239.
[51] Visaria, M., Mudawar, I., and Pourpoint, T., 2001, "Enhanced Heat Exchanger Design for Hydrogen Storage Using High-Pressure Metal Hydride—Part 1. Design Methodology and Computational Results," Int. J. Heat Mass Transfer, **54**, pp. 413–423.
[52] Visaria, M., Mudawar, I., and Pourpoint, T., 2001, "Enhanced Heat Exchanger Design for Hydrogen Storage Using High-Pressure Metal Hydride—Part 2. Experimental Methods," Int. J. Heat Mass Transfer, **54**, pp. 424–432.
[53] Mudawar, I., 2009, "Micro-Channel Heat Exchangers for Metal Hydride Hydrogen Storage Systems," U.S. Provisional Patent Application No. 61/184,595.
[54] Kirschman, R. K., 1985, "Cold Electronics: An Overview," Cryogenics, **25**, pp. 115–122.
[55] Phelan, P. E., Chiriac, V. A., and Lee, T.-Y. T., 2002, "Current and Future Miniature Refrigeration Cooling Technologies for High Power Microelectronics," IEEE Trans. Compon. Packag. Manuf. Technol., **25**, pp. 356–365.
[56] Peeples, J. W., Little, W., Schmidt, R., and Nisenoff, M., 2000, "Low Temperature Electronics Workshop," *Proceedings of the 16th Semiconductor Thermal Measurement and Management Symposium*, San Jose, CA, pp. 108–109.
[57] Schmidt, R. R., and Notohardjono, B. D., 2002, "High-End Server Low-Temperature Cooling," IBM J. Res. Dev., **46**, pp. 739–751.
[58] Chiriac, V., and Chiriac, F., 2006, "The Optimization of a Refrigerant Vapor Compression System for Power Microelectronics," *Proceedings of the ITherm 2006*, San Diego, CA, pp. 759–764.
[59] Wadell, R., Joshi, Y. K., and Fedorov, A. G., 2007, "Experimental Investigation of Compact Evaporators for Ultralow Temperature Refrigeration of Microprocessors," ASME J. Electron. Packag., **129**, pp. 291–299.
[60] Tran, T. N., Chyu, M.-C., Wambsganss, M. W., and France, D. M., 2000, "Two-Phase Pressure Drop of Refrigerants During Flow Boiling in Small Channels: An Experimental Investigation and Correlation Development," Int. J. Multiphase Flow, **26**, pp. 1739–1754.
[61] Lee, H. J., and Lee, S. Y., 2001, "Pressure Drop Correlations for Two-Phase Flow Within Horizontal Rectangular Channels With Small Heights," Int. J. Multiphase Flow, **27**, pp. 783–796.
[62] Qu, W., and Mudawar, I., 2003, "Flow Boiling Heat Transfer in Two-Phase Micro-Channel Heat Sinks—I. Experimental Investigation and Assessment of Correlation Methods," Int. J. Heat Mass Transfer, **46**, pp. 2755–2771.
[63] Qu, W., and Mudawar, I., 2003, "Flow Boiling Heat Transfer in Two-Phase Micro-Channel Heat Sinks—II. Annular Two-Phase Flow Model," Int. J. Heat Mass Transfer, **46**, pp. 2773–2784.
[64] Lee, J., and Mudawar, I., 2005, "Two-Phase Flow in High-Heat-Flux Micro-Channel Heat Sink for Refrigeration Cooling Applications: Part I—Pressure Drop Characteristics," Int. J. Heat Mass Transfer, **48**, pp. 928–940.
[65] Lee, J., and Mudawar, I., 2005, "Two-Phase Flow in High-Heat-Flux Micro-Channel Heat Sink for Refrigeration Cooling Applications: Part II—Heat Transfer Characteristics," Int. J. Heat Mass Transfer, **48**, pp. 928–940.
[66] Lee, J., and Mudawar, I., 2008, "Fluid Flow and Heat Transfer Characteristics of Low Temperature Two-Phase Micro-Channel Heat Sinks—Part 1: Experimental Methods and Flow Visualization Results," Int. J. Heat Mass Transfer, **51**, pp. 4315–4326.
[67] Lee, J., and Mudawar, I., 2008, "Fluid Flow and Heat Transfer Characteristics of Low temperature Two-Phase Micro-Channel Heat Sinks—Part 2: Subcooled Boiling Pressure Drop and Heat Transfer," Int. J. Heat Mass Transfer, **51**, pp. 4327–4341.
[68] Lee, J., and Mudawar, I., 2009, "Critical Heat Flux for Subcooled Flow Boiling in Micro-Channel Heat Sinks," Int. J. Heat Mass Transfer, **52**, pp. 3341–3352.
[69] Lee, J., and Mudawar, I., 2009, "Experimental Investigation and Theoretical Model for Subcooled Flow Boiling Pressure Drop in Micro-Channel Heat Sinks," ASME J. Electron. Packag., **131**, 031008.
[70] Lee, J., and Mudawar, I., 2009, "Low-Temperature Two-Phase Micro-Channel Cooling for High-Heat-Flux Thermal Management of Defense Electronics," IEEE Trans. Compon. Packag. Manuf. Technol., **32**, pp. 453–465.
[71] Chiaramonte, F. P., and Joshi, J. A., 2004, "Workshop on Critical Issues in Microgravity Fluids, Transport, and Reaction Processes in Advanced Human Support Technology—Final Report," Report No. NASA TM-2004-212940.
[72] Zhang, H., I. Mudawar, I., and Hasan, M. M., 2005, "Flow Boiling CHF in Microgravity," Int. J. Heat Mass Transfer, **48**, pp. 3107–3118.
[73] Saito, M., Yamaoka, N., Miyazaki, K., Kinoshita, M., and Abe, Y., 1994, "Boiling Two-Phase Flow Under Microgravity," Nucl. Eng. Des., **146**, pp. 451–461.
[74] Cochran, T. H., 1970, "Forced-Convection Boiling Near Inception in Zero-Gravity," NASA Technical Note D-5612.
[75] Ma, Y., and Chung, J. N., 2001, "An Experimental Study of Critical Heat Flux (CHF) in Microgravity Forced-Convection Boiling," Int. J. Multiphase Flow, **27**, pp. 1753–1767.
[76] Zhang, H., Mudawar, I., and Hasan, M. M., 2007, "Assessment of Dimensionless CHF Correlations for Subcooled Flow Boiling in Microgravity and Earth Gravity," Int. J. Heat Mass Transfer, **50**, pp. 4568–4580.
[77] Zhang, H., Mudawar, I., and Hasan, M. M., 2004, "A Method for Assessing the Importance of Body Force on Flow Boiling CHF," ASME J. Heat Transfer, **126**, pp. 161–168.
[78] Zhang, H., Mudawar, I., and Hasan, M. M., 2009, "Application of Flow Boiling for Thermal Management of Electronics in Microgravity and Reduced Gravity Systems," IEEE Trans. Compon. Packag. Manuf. Technol., **32**, pp. 466–477.
[79] Ku, J., 1993, "Overview of Capillary Pumped Loop Technology," *Proceedings of the 29th National Heat Transfer Conference*, ASME, Atlanta, GA, HTD-Vol. 236, pp. 1–17.
[80] LaClair, T. J., and Mudawar, I., 2000, "Thermal Transients in a Capillary Evaporator Prior to the Initiation of Boiling," Int. J. Heat Mass Transfer, **43**, pp. 3937–3952.
[81] Cullimore, B. A., 1991, "Start Up Transients in Capillary Pumped Loops," AIAA Paper No. 91-1374, Reston, VA.
[82] LaClair, T. J., and Mudawar, I., 2009, "Theoretical Model for Fast Bubble Growth in Small Channels With Reference to Startup of Capillary Pumped Loops Used in Spacecraft Thermal Management Systems," Int. J. Heat Mass Transfer, **52**, pp. 716–723.
[83] Mala, G. M., and Li, D., 1999, "Flow Characteristics of Water in Microtubes," Int. J. Heat Fluid Flow, **20**, pp. 142–148.
[84] Papautsky, I., Brazzle, J., Ameel, T., and Frazier, A. B., 1999, "Laminar Fluid Behavior in Microchannels Using Micropolar Fluid Theory," Sens. Actuators, A, **73**, pp. 101–108.
[85] Choi, S. B., Barron, R. R., and Warrington, R. O., 1991, "Fluid Flow and Heat Transfer in Micro Tubes," ASME DSC-40, pp. 89–93.
[86] Peng, X. F., Peterson, G. P., and Wang, B. X., 1994, "Frictional Flow Characteristics of Water Flowing Through Rectangular Microchannels," Exp. Heat Transfer, **7**, pp. 249–264.
[87] Flockhart, S. M., and Dhariwal, R. S., 1998, "Experimental and Numerical Investigation Into the Flow Characteristics of Channels Etched in <100> Silicon," ASME J. Fluids Eng., **120**, pp. 291–295.
[88] Judy, J., Maynes, D., and Webb, B. W., 2002, "Characterization of Frictional Pressure Drop for Liquid Flows Through Microchannels," Int. J. Heat Mass Transfer, **45**, pp. 3477–3489.
[89] Wu, H. Y., and Cheng, D., 2003, "Friction Factors in Smooth Trapezoidal Silicon Microchannels With Different Aspect Ratios," Int. J. Heat Mass Transfer, **46**, pp. 2519–2525.
[90] Qu, W., Mudawar, I., Lee, S.-Y., and Wereley, S. T., 2006, "Experimental and Computational Investigation of Flow Development and Pressure Drop in a Rectangular Micro-Channel," ASME J. Electron. Packag., **128**, pp. 1–9.
[91] Gan, Y., Xu, J., and Wang, S., 2008, "Are the Available Boiling Heat Transfer Coefficients Suitable for Silicon Microchannel Heat Sinks?," Microfluids Nanofluids, **4**, pp. 575–587.
[92] Hetsroni, G., Mosyak, A., Pogrebnyak, E., and Segal, Z., 2006, "Periodic Boiling in Parallel Micro-Channels at Low Vapor Quality," Int. J. Multiphase Flow, **32**, pp. 1141–1159.
[93] Wang, G., Cheng, P., and Bergles, A. E., 2008, "Effects of Inlet/Outlet Configurations on Flow Boiling Instability in Parallel Microchannels," Int. J. Heat Mass Transfer, **51**, 2267–2281.
[94] Wu, H. Y., and Cheng, P., 2004, "Boiling Instability in Parallel Silicon Microchannels at Different Heat Flux," Int. J. Heat Mass Transfer, **47**, pp. 3631–3641.
[95] Jiang, L., Wong, M., and Zohar, Y., 1999, "Phase Change in Microchannel Heat Sinks With Integrated Temperature Sensors," J. Microelectromech. Syst., **8**, pp. 358–365.
[96] Cortés, C., Diez, L. I., and Campo, A., 2008, "Efficiency of Composite Fins of Variable Thickness," Int. J. Heat Mass Transfer, **51**, pp. 2153–2166.
[97] Kim, S. M., and Mudawar, I., 2010, "Analytical Heat Diffusion Models for Different Micro-Channel Heat Sink Cross-Sectional Geometries," Int. J. Heat Mass Transfer, **53**, pp. 4001–4016.
[98] Kim, S. M., and Mudawar, I., 2010, "Analytical Heat Diffusion Models for Heat Sinks With Circular Micro-Channels," Int. J. Heat Mass Transfer, **53**, pp. 4552–4566.
[99] Thome, J. R., 2004, "Boiling in Microchannels: A Review of Experiment and Theory," Heat Fluid Flow, **25**, pp. 128–139.
[100] Liao, S.-J., 2002, "An Analytic Approximation of the Drag Coefficient for the Viscous Flow Past a Sphere," Int. J. Non-Linear Mech., **37**, pp. 1–18.
[101] Sato, T., and Matsumura, H., 1963, "On the Conditions of Incipient Subcooled Boiling and Forced-Convection," Bull. JSME, **7**, pp. 392–398.
[102] Davis, E. J., and Anderson, G. H., 1966, "The Incipience of Nucleate Boiling in Forced Convection Flow," AIChE J., **12**, pp. 774–780.
[103] Qu, W., and Mudawar, I., 2002, "Prediction and Measurement of Incipient Boiling Heat Flux in Micro-Channel Heat Sinks," Int. J. Heat Mass Transfer, **45**, pp. 3933–3945.
[104] Qu, W., and Mudawar, I., 2003, "Thermal Design Methodology for High-Heat-Flux Single-Phase and Two-Phase Micro-Channel Heat Sinks," IEEE Trans. Compon. Packag. Manuf. Technol., **26**, pp. 598–609.
[105] Al-Hayes, R. A. M., and Winterton, R. H. S., 1981, "Bubble Diameter in Detachment in Flowing Liquids," Int. J. Heat Mass Transfer, **24**, pp. 223–230.
[106] Winterton, R. H. S., 1984, "Flow Boiling: Prediction of Bubble Departure," Int. J. Heat Mass Transfer, **27**, pp. 1422–1424.
[107] Willingham, T. C., and Mudawar, I., 1992, "Channel Height Effects on Forced-Convection Boiling and Critical Heat Flux From a Linear Array of Discrete Heat Sources," Int. J. Heat Mass Transfer, **35**, pp. 1865–1880.
[108] Willingham, T. C., and Mudawar, I., 1992, "Forced-Convection Boiling and Critical Heat Flux From a Linear Array of Discrete Heat Sources," Int. J. Heat Mass Transfer, **35**, pp. 2879–2890.

[109] Hosler, E. R., 1968, "Flow Patterns in High Pressure Two-Phase (Steam-Water) Flow With Heat Addition," AIChE Symp. Ser., **64**, pp. 54–66.
[110] Wambsganss, M. W., Jendrzejczyk, J. A., and France, D. M., 1991, "Two-Phase Flow Patterns and Transition in a Small, Horizontal, Rectangular Channel," Int. J. Multiphase Flow, **17**, pp. 327–342.
[111] Ali, M. I., and Kawaji, M., 1991, "The Effect of Flow Channel Orientation on Two-Phase Flow in a Narrow Passage Between Flat Plates," *Proceedings of the 1991 ASME/JSME Thermal Engineering Joint Conference*, J. R. Lloyd and Y. Kurosaki, eds., ASME, New York, NY, Vol. 2, pp. 183–190.
[112] Mishima, K., Hibiki, T., and Nishihara, H., 1993, "Some Characteristics of Gas-Liquid Flow in Narrow Rectangular Ducts," Int. J. Multiphase Flow, **19**, pp. 115–124.
[113] Fujita, H., Ohara, T., Hirota, M., and Furuta, H., 1995, "Gas-Liquid Flows in Flat Channels With Small Channel Clearance," *Advances in Multiphase Flow*, A. Serizawa, T. Fukano, and J. Bataille, eds., Elsevier, New York, NY, pp. 441–451.
[114] Xu, J. L., Cheng, P., and Zhao, T. S., 1999, "Gas-Liquid Two-Phase Flow Regimes in Rectangular Channels With Mini/Micro Gaps," Int. J. Multiphase Flow, **25**, pp. 411–432.
[115] Qu, W., Yoon, S.-M., and Mudawar, I., 2004, "Two-Phase Flow and Heat Transfer in Rectangular Micro-Channels," ASME J. Electron. Packag., **126**, pp. 288–300.
[116] Mandhane, J. M., Gregory, G. A., and Aziz, K., 1974, "A Flow Pattern Map for Gas-Liquid Flow in Horizontal Pips," Int. J. Multiphase Flow, **1**, pp. 537–553.
[117] Taitel, Y., and Dukler, A. E., 1976, "A Model for Predicting Flow Regime Transitions in Horizontal and Near Horizontal Gas-Liquid Flow," AIChE J., **22**, pp. 47–55.
[118] Bergles, A. E., 1977, "Review of Instability in Two-Phase Systems," *Two-Phase Flows and Heat Transfer*, S. Kakac, and F. Mayinger, eds., Hemisphere, Washington, Vol. 1, pp. 383–422.
[119] Yadigaroglu, G., 1981, "Two-Phase Flow Instabilities and Propagation Phenomena," *Thermohydraulics of Two-Phase Systems for Industrial Design and Nuclear Engineering*, J. M. Delhaye, M. Giot, and M. L. Riethmuller, eds., Hemisphere, Washington, pp. 353–403.
[120] Qu, W., and Mudawar, I., 2003, "Measurement and Prediction of Pressure Drop in Two-Phase Micro-Channel Heat Sinks," Int. J. Heat Mass Transfer, **46**, pp. 2737–2753.
[121] Shah, R. K., and London, A. L., 1978, *Laminar Flow Forced Convection in Ducts: A Source Book for Compact Heat Exchanger Analytical Data, Supplement 1*, Academic, New York, NY.
[122] Lee, J., 2008, "Investigation of Subcooled Boiling in Micro-Channel Heat Sink for Indirect Refrigeration Cooling Applications," Ph.D. thesis, Purdue University, West Lafayette, IN.
[123] McAdams, W. H., Woods, W. K., and Heroman, L. C., 1942, "Vaporization Inside Horizontal Tubes, II. Benzene-Oil Mixture," Trans. ASME, **64**, pp. 193–200.
[124] Davidson, W. F., Hardie, P. H., Humphreys, C. G. R., Markson, A. A., Mumford, A. R., and Ravese, T., 1943, "Studies of Heat Transmission Through Boiler Tubing at Pressures From 500 to 3300 Pounds," Trans. ASME, **65**, pp. 553–591.
[125] Cicchitti, A., Lombardi, C., Silvestri, M., Soldaini, G., and Zavalluilli, R., 1960, "Two-Phase Cooling Experiments-Pressure Drop, Heat Transfer and Burnout Measurements," Energ. Nucl., **7**, pp. 407–425.
[126] Owens, W. L., 1961, "Two-Phase Pressure Gradient," Int. Dev. Heat Transfer, Part II, ASME, pp. 363–368.
[127] Dukler, A. E., Wicks, M., and Cleaveland, R. G., 1964, "Pressure Drop and Hold Up in Two-Phase Flow," AIChE J., **10**, pp. 38–51.
[128] Zivi, S. M., 1964, "Estimation of Steady-State Steam Void-Fraction by Means of the Principle of Minimum Entropy Production," ASME J. Heat Transfer, **86**, pp. 247–252.
[129] Lockhart, R. W., and Martinelli, R. C., 1949, "Proposed Correlation of Data for Isothermal Two-Phase, Two-Component Flow in Pipes," Chem. Eng. Prog., **45**, pp. 39–48.
[130] Mishima, K., and Hibiki, T., 1996, "Some Characteristics of Air–Water Two-Phase Flow in Small Diameter Vertical Tubes," Int. J. Multiphase Flow, **22**, pp. 703–712.
[131] Blevins, R. D., 1984, *Applied Fluid Dynamics Handbook*, Van Nostrand Reinhold, New York, NY.
[132] Collier, J. G., and Thome, J. R., 1994, *Convective Boiling and Condensation*, 3rd ed., Oxford University Press, New York, NY.
[133] Copeland, D., 1995, "Manifold Microchannel Heat Sinks: Analysis and Optimization," Therm. Sci. Eng., **3**, pp. 7–12.
[134] Al-Arabi, M., 1982, "Turbulent Heat Transfer in the Entrance Region of a Tube," Heat Transfer Eng., **3**, pp. 76–83.
[135] Chen, J. C., 1966, "Correlation for Boiling Heat Transfer to Saturated Fluids in Convective Flow," I&EC Process Des. Dev., **5**, pp. 322–329.
[136] Shah, M. M., 1982, "Chart Correlation for Saturated Boiling Heat Transfer: Equation and Further Study," ASHRAE Trans., **88**, pp. 185–196.
[137] Gungor, K. E., and Winterton, R. H. S., 1986, "A General Correlation for Flow Boiling in Tubes and Annuli," Int. J. Heat Mass Transfer, **29**, pp. 351–358.
[138] Kandlikar, S. G., 1990, "A General Correlation for Saturated Two-Phase Flow Boiling Heat Transfer Inside Horizontal and Vertical Tubes," ASME J. Heat Transfer, **112**, pp. 219–228.
[139] Liu, Z., and Winterton, R. H. S., 1991, "A General Correlation for Saturated and Subcooled Flow Boiling in Tube and Annuli," Int. J. Heat Mass Transfer, **34**, pp. 2759–2766.
[140] Steiner, D., and Taborek, J., 1992, "Flow Boiling Heat Transfer in Vertical Tubes Correlated by an Asymptotic Model," Heat Transfer Eng., **13**, pp. 43–69.
[141] Lazarek, G. M., and Black, S. H., 1982, "Evaporative Heat Transfer, Pressure Drop and Critical Heat Flux in a Small Vertical Tube With R-113," Int. J. Heat Mass Transfer, **25**, pp. 945–959.
[142] Tran, T. N., Wambsganss, M. W., and France, D. M., 1996, "Small Circular- and Rectangular-Channel Boiling With Two Refrigerants," Int. J. Multiphase Flow, **22**, pp. 485–498.
[143] Lee, H. J., and Lee, S. Y., 2001, "Heat Transfer Correlation for Boiling Flows in Small Rectangular Horizontal Channels With Low Aspect Ratios," Int. J. Multiphase Flow, **27**, pp. 2043–2062.
[144] Yu, W., France, D. M., Wambsganss, M. W., and Hull, J. R., 2002, "Two-Phase Pressure Drop, Boiling Heat Transfer, and Critical Heat Flux to Water in a Small-Diameter Horizontal Tube," Int. J. Multiphase Flow, **28**, pp. 927–941.
[145] Warrier, G. R., Dhir, V. K., and Momoda, L. A., 2002, "Heat Transfer and Pressure Drop in Narrow Rectangular Channels," Exp. Therm. Fluid Sci., **26**, pp. 53–64.
[146] Katto, Y., and Ohno, H., 1984, "An Improved Version of the Generalized Correlation of Critical Heat Flux for the Forced Convective Boiling in Uniformly Heated Vertical Tubes," Int. J. Heat Mass Transfer, **27**, pp. 1641–1648.
[147] Hall, D. D., and Mudawar, I., 2000, "Critical Heat Flux (CHF) for Water Flow in Tubes—I. Compilation and Assessment of World CHF Data," Int. J. Heat Mass Transfer, **43**, pp. 2573–2604.
[148] Hall, D. D., and Mudawar, I., 2000, "Critical Heat Flux (CHF) for Water Flow in Tubes-II. Subcooled CHF Correlations," Int. J. Heat Mass Transfer, **43**, pp. 2605–2640.
[149] Qu, W., and Mudawar, I., 2005, "A Systematic Method for Optimal Design of Two-Phase Micro-Channel Heat Sinks," ASME J. Electron. Packag., **127**, pp. 381–390.
[150] Lee, J., and Mudawar, I., 2006, "Implementation of Micro-Channel Evaporator for High-Heat-Flux Refrigeration Cooling Applications," ASME J. Electron. Packag., **128**, pp. 30–37.
[151] Choi, S. U. S., 1995, "Enhancing Thermal Conductivity of Fluids With Nanoparticles," *Developments and Applications of Non-Newtonian Flows*, D. A. Siginer and H. P. Wang, eds., ASME, New York, NY, FED-Vol. 231/MD-Vol. 66, pp. 99–105.
[152] Lee, S., Choi, S. U.-S., Li, S., and Eastman, J. A., 1999, "Measuring Thermal Conductivity of Fluids Containing Oxide Nanoparticles," ASME J. Heat Transfer, **121**, pp. 280–289.
[153] Xue, Q.-Z., 2003, "Model for Effective Thermal Conductivity of Nanofluids," Phys. Lett. A, **307**, pp. 313–317.
[154] Lee, J., and Mudawar, I., 2007, "Assessment of the Effectiveness of Nanofluids for Single-Phase and Two-Phase Heat Transfer in Micro-Channels," Int. J. Heat Mass Transfer, **50**, pp. 452–463.
[155] Kim, P., Shi, L., Majumdar, A., and McEuen, P. L., 2001, "Thermal Transport Measurements of Individual Multiwalled Nanotubes," Phys. Rev. Lett., **87**, pp. 1–4.
[156] Ujereh, S., Fisher, T., and Mudawar, I., 2007, "Effects of Carbon Nanotube Arrays on Nucleate Pool Boiling," Int. J. Heat Mass Transfer, **50**, pp. 4023–4038.
[157] Launay, S., Fedorov, A. G., Joshi, Y., Cao, A., and Ajayan, P. M., 2006, "Hybrid Micro-Nano Structured Thermal Interfaces for Pool Boiling Heat Transfer Enhancement," Microelectron. J., **37**, pp. 1158–1164.
[158] Khanikar, V., Mudawar, I., and Fisher, T., 2009, "Effects of Carbon Nanotube Coating on Flow Boiling in a Micro-Channel," Int. J. Heat Mass Transfer, **52**, pp. 3805–3817.
[159] Anderson T. M., and Mudawar, I., 1989, "Microelectronic Cooling by Enhanced Pool Boiling of a Dielectric Fluorocarbon Liquid," ASME J. Heat Transfer, **111**, pp. 752–759.
[160] Mukherjee, S., and Mudawar, I., 2003, "Smart, Low-Cost, Pumpless Loop for Micro-Channel Electronic Cooling Using Flat and Enhanced Surfaces," IEEE Trans. Compon. Packag. Manuf. Technol., **26**, pp. 99–109.
[161] Mukherjee, S., and Mudawar, I., 2003, "Pumpless Loop for Narrow Channel and Micro-Channel Boiling From Vertical Surfaces," ASME J. Electron. Packag., **125**, pp. 431–441.
[162] Mudawar, I., and Wadsworth, D. C., 1991, "Critical Heat Flux From a Simulated Electronic Chip to a Confined Rectangular Impinging Jet of Dielectric Liquid," Int. J. Heat Mass Transfer, **34**, pp. 1465–1480.
[163] Wadsworth, D. C., and Mudawar, I., 1992, "Enhancement of Single-Phase Heat Transfer and Critical Heat Flux From an Ultra-High-Flux Simulated Microelectronic Heat Source to a Rectangular Impinging Jet of Dielectric Liquid," ASME J. Heat Transfer, **114**, pp. 764–768.
[164] Sung, M. K., and Mudawar, I., 2008, "Single-Phase and Two-Phase Cooling Using Hybrid Micro-Channel/Slot-Jet Module," Int. J. Heat Mass Transfer, **51**, pp. 3825–3839.
[165] Sung, M. K., and Mudawar, I., 2009, "Effects of Jet Pattern on Two-Phase Cooling Performance of Hybrid Micro-Channel/Micro-Circular-Jet-Impingement Thermal Management Scheme," Int. J. Heat Mass Transfer, **52**, pp. 3364–3372.
[166] Sung, M. K., and Mudawar, I., 2009, "CHF Determination for High-Heat-Flux Phase-Change Cooling System Incorporating Both Micro-Channel Flow and Jet-Impingement," Int. J. Heat Mass Transfer, **52**, pp. 610–619.
[167] Sung, M. K., and Mudawar, I., 2009, "Single-Phase and Two-Phase Hybrid Cooling Scheme for High-Heat-Flux Thermal Management of Defense Electronics," ASME J. Electron. Packag., **131**, 021013.
[168] Ndao, S., Peles, Y., and Jensen, M. K., 2009, "Multi-Objective Thermal Design Optimization and Comparative Analysis of Electronics Cooling Technologies," Int. J. Heat Mass Transfer, **52**, pp. 4317–4326.